Estuaries and Coasts (2022) 45:1780–1802
https://doi.org/10.1007/s12237-021-01041-x

Sr Isotope Ratios ($^{87}Sr/^{86}Sr$) in Water and Fish Otoliths as Estuarine Salinity Tracers: Case Studies from Three NW African Rivers

Sebastian N. Höpker[1,2,3] · Henry C. Wu[1] · Friedrich Lucassen[4] · Oumar Sadio[5] · Timothée Brochier[6,7] · Ishmael Y. Nuworkpor[8] · Simone A. Kasemann[4] · Peter Merschel[1,9] · Hildegard Westphal[1,2,10]

Received: 14 June 2021 / Revised: 22 November 2021 / Accepted: 15 December 2021 / Published online: 4 February 2022

Abstract

Variations of strontium isotope ratios ($^{87}Sr/^{86}Sr$) in river systems are increasingly utilised to geochemically trace origin and movement patterns of migratory fish species. Accretionary calcified structures, such as otoliths, preserve $^{87}Sr/^{86}Sr$ signatures of the surrounding water during a fish's lifetime. In this study, we present $^{87}Sr/^{86}Sr$ measurements of water samples and catfish otoliths collected in the estuaries of the Sine-Saloum (Senegal), the Gambia River (The Gambia), and the Volta River (Ghana) to assess their systematics and relationships with salinity. The three rivers possess distinct hydrological properties resulting in variable degrees of correlations between $^{87}Sr/^{86}Sr$ and salinity. The Gambia River ($^{87}Sr/^{86}Sr$ of ~ 0.71209) proved exceptionally preconditioned for the approach due to well-defined geochemical end-members, allowing for quantitative estimates of salinity based on otolith $^{87}Sr/^{86}Sr$ measurements. The Volta River (~ 0.71392) presents a more complex case due the possible influence of multiple water sources to the main channel, while the inverse salinity gradient and excessive evaporation in the Sine-Saloum estuary (~0.70915) impede any significant correlations between $^{87}Sr/^{86}Sr$ and salinity. Bulk otolith $^{87}Sr/^{86}Sr$ values in the Gambia River and Volta River clearly depicted a mixed influence of seawater and riverine compositions, strongly encouraging the application of this approach for geochemical fingerprinting of critical NW African species.

Keywords Strontium · Salinity · Hydrochemistry · Carbonate · Catfish · West Africa

Introduction

Strontium isotope ratios ($^{87}Sr/^{86}Sr$) preserved in natural materials reflect the available Sr sources during their formation, enabling the use of $^{87}Sr/^{86}Sr$ signatures as chemical tracers for a range of applications. Traditionally a tool for geological provenance studies (Meyer et al. 2011; Zhao et al. 2018) and chronostratigraphy in marine sediments (Marcano et al. 2009; Veizer et al. 1999), geochemical "fingerprinting" based on $^{87}Sr/^{86}Sr$ is increasingly utilised in other disciplines, such as fisheries and (palaeo-)ecology studies

Communicated by Jill A. Olin

✉ Sebastian N. Höpker
seb.hoepker@gmail.com

✉ Henry C. Wu
henry.wu@leibniz-zmt.de

1 Leibniz Centre for Tropical Marine Research (ZMT) GmbH, Bremen, Germany

2 Faculty of Geosciences, University of Bremen, Bremen, Germany

3 Present Address: Environmental Research Institute, School of Science, Faculty of Science and Engineering, University of Waikato, Hamilton, New Zealand

4 Faculty of Geosciences and MARUM – Center for Marine Environmental Sciences, University of Bremen, Bremen, Germany

5 Institute for Development (IRD), UMR LEMAR 195 (Environmental Sciences Laboratory MARin), Dakar, Senegal

6 Institute for Development (IRD), Sorbonne Université (SU), UMMISCO, 93143 Bondy, France

7 Institute for Development (IRD), Université Cheikh Anta Diop (UCAD), Ecole Supérieur Polytechnique (ESP), UMMISCO, Dakar, Senegal

8 Takoradi Technical University, Takoradi, Ghana

9 Current Address: BDG Berufsverband Deutscher Geowissenschaftler E.V, Bonn, Germany

10 King Abdullah University of Science and Technology (KAUST), Thuwal, Saudi Arabia

(Crowley et al. 2017), archaeology (Hodell et al. 2004), or forensics (Beard and Johnson 2000; DeBord et al. 2017).

The marine Sr budget and isotopic composition of seawater varied during Earth's history in response to climatic and/or tectonic forcings that largely control the supply and geochemistry of continental inputs (Banner 2004; Jones et al. 2014; McArthur et al. 2001; Mokadem et al. 2015). The residence time of Sr (~2–5 × 10^6 years) greatly exceeds the time it takes for the world oceans to mix (~10^3 years; Burke et al. 1982; Veizer et al. 1999). Therefore, the Sr isotopic composition of seawater is globally highly homogeneous at any given time. The modern $^{87}Sr/^{86}Sr$ value of approximately 0.70918 ± 0.00001 (2σ; Faure and Mensing 2005), which presents a more conservative estimate representative of a wide range of measurements from different oceanic regions with variable analytical precision (e.g., Ando et al. 2010; Elderfield 1986; El Meknassi et al. 2018; Farrell et al. 1995; McArthur et al. 2001; Mokadem et al. 2015), has not significantly changed over the past ~40,000 years (Mokadem et al. 2015).

In marginal seas, the $^{87}Sr/^{86}Sr$ values of water may locally vary as a result of mixing of seawater with continental runoff (Huang et al. 2011). While the Sr content is also dependent on the water chemistry and available ligands, both the Sr concentration and the isotopic composition of riverine waters are at large governed by the drainage basin lithology and temporal variations in weathering rates (Blum and Erel 2003). Importantly, Sr and $^{87}Sr/^{86}Sr$ typically exhibit near-conservative mixing behaviour allowing for the establishment of quantitative relationships between these parameters and salinity along estuarine gradients (e.g., Hobbs et al. 2019; Ingram and Sloan 1992; Peros et al. 2007; Widerlund and Andersson 2006; Wierzbowski 2013). Such mixing lines can in turn be used to infer salinity histories based on Sr isolated from calcareous skeletal materials, e.g., fish otoliths, of estuarine calcifying organisms. Bioavailable Sr is readily incorporated into the crystal structure of calcium carbonate because Sr^{2+} and Ca^{2+} ions have the same valence and similar ionic radius (1.18 Å and 1.00 Å for Sr and Ca cations, respectively; Capo et al. 1998). However, the Sr/Ca ratios in fish otoliths and bivalve shells depend on multiple complex controls during the precipitation of aragonite that significantly limit their applicability as environmental proxies (Elliot et al. 2009; Gillikin et al. 2005; Poulain et al. 2015). These controls include effects of water chemistry and salinity, temperature, and various physiological processes (Campana 1999; Freitas et al. 2006; Mohan et al. 2012; Panfili et al. 2015), some of which may be species-specific (Chang et al. 2004; Gillikin et al. 2005). In contrast, $^{87}Sr/^{86}Sr$ values are not subject to any significant fractionation during the precipitation of biogenic carbonates due to their relatively large atomic mass and directly reflect the composition of the surrounding water (Flockhart et al. 2015; Liu et al. 2015; Palmer and Edmond 1989; Reinhardt et al. 1998).

Presently, there are limited accounts of $^{87}Sr/^{86}Sr$ systematics in NW African estuaries with exception of few measurements in the lower Volta River estuary in Ghana (Jørgensen and Banoeng-Yakubo 2001) and the coastal Oualidia Lagoon in Morocco (El Meknassi et al. 2020). Models aiming to constrain the contribution from NW Africa to the global marine Sr budget thus rely entirely on estimates of both Sr concentrations and isotopic ratios based on the dominant catchment lithology of the region. In contrast to river water analyses, such model estimates do not account for potentially altered aqueous element budgets. For instance, the Senegal River and the Casamance in southern Senegal present NW African examples of systems substantially modified from their natural state through extensive land-use changes, anthropogenic inputs across their catchment, and climatic extremes (Degeorges and Reilly 2006; Barusseau et al. 1998; Simier et al. 2006). Moreover, the paucity of information on the geochemical properties of modern continental runoff along the NW African coast restricts the potential of palaeoenvironmental applications, such as tracing the temporal patterns in riverine discharge to inform past hydroclimate variability (e.g., Höpker et al. 2019 (Banc d'Arguin, Mauritania), Ingram and Sloan 1992 (San Francisco Bay, USA), Peros et al. 2007 (Laguna de la Leche, Cuba)).

This study provides the first measurements of Sr concentrations and $^{87}Sr/^{86}Sr$ in three selected systems with varying hydrological properties from NW Africa. The Gambia River (The Gambia) is one of very few remaining aquatic ecosystems in West Africa that has not been strongly modified by anthropogenic disturbances, and as such presents a rare example of a rather natural riverine system in this region (Sarré et al. 2018; Simier et al. 2006). Notwithstanding its similarly pristine ecological state, the nearby Sine-Saloum in Senegal presents a stark contrast with an inverse salinity gradient caused by excessive evaporation over recent decades. Finally, we present data from the Lower Volta River in Ghana, the terminus of one of the largest fluvial networks in West Africa. Despite vastly altered in flow by the Akosombo dam, knowledge of the Sr geochemistry of modern outflow from the Volta River is highly relevant to the ongoing revision of the marine Sr budget (Beck et al. 2013; Peucker-Ehrenbrink and Fiske 2019).

Various economically significant catfish species targeted by both industrial and artisanal fisheries are common to these estuaries, including the Guinean sea catfish (*Carlarius parkii*; Günther 1864) and Bagrid catfish (*Chrysichthys nigrodigitatus*; Lacepède 1803). *C. parkii* are a demersal and marine-estuarine generalist predatory species that reproduces at sea, but otherwise regularly inhabits the brackish waters of estuaries and coastal lagoons between Mauritania and Angola (Marceniuk and Menezes 2007; Schneider 1990; Simier et al. 2021; Taylor 1986). Juvenile and adult *C. parkii* move relatively freely through estuaries and are found as

far as ~190 km upstream in the Gambia River (Laë et al. 2004), while salinities exceeding 50 restrict their presence to the lower ~ 30 km of the adjacent Sine-Saloum (Panfili et al. 2006; Simier et al. 2021). Along with other Ariidae, *C. parkii* form a major component of fisheries along the Senegalese and Gambian coast (Ba et al. 2018; Laë et al. 2004), while also highly impacted by bycatch (e.g., Castro et al. 2013). *C. nigrodigitatus* are of freshwater origin and common to most western African basins, primarily inhabiting the shallow waters of lakes, rivers and swamps. Although considered potamodromous, they also frequent the estuarine waters of the lower Volta River and adjacent brackish lagoons (Dankwa and Gordon 2002). However, catch numbers from the nearby Pra River estuary (Ghana) decrease with higher salinity and turbidity, suggesting that movements towards brackish waters are likely short-lived and driven by a greater diversity in food sources for the demersal omnivores (Okyere and Boahemaa-Kobil 2020). Despite their economic importance, a lack of tagging or chemical tracing studies of Ariidae and *Chrysichthys* spp. limits our knowledge of specific migration patterns and habitat use that may be critical in better constraining population dynamics.

In this study, we assess the potential in each of the three estuaries for establishing quantitative relationships between water $^{87}Sr/^{86}Sr$ and salinity. With view to facilitating geochemical provenance studies of key aquatic species, we include exemplary salinity reconstructions based on *C. parkii* and *C. nigrodigitatus* otoliths collected from each estuary. The study further aims to provide modern reference to extend the record of historical salinity and discharge patterns through archaeological carbonate deposits ubiquitous to the NW African coast. At large, our results aid in refining the marine Sr budget, while also presenting fundamental data relevant to a range of geological, archaeological and ecological applications.

Material and Methods

Study Areas

The Gambia River, The Gambia

The Gambia River (Fig. 1a) originates from the Fouta Djalon plateau in northern Guinea, from which it flows ~1200 km through Guinea, Senegal, and The Gambia, draining a catchment area of ~78,000 km^2 primarily comprised of lowlands. The lower part of the river consists of a single main channel lined by tidal floodplains and mangrove swamps (Mikhailov and Isupova 2008), and discharges into the Atlantic Ocean at ca. 13° 30′ 22″ N, 16° 34′ 58″ W. The climate is Sahelo-Sudanian with a wet season from June to October and a dry season from November to May (Simier et al. 2006), and an annual precipitation of 1100 to 1500 mm (Mikhailov and Isupova 2008). The estuarine zone generally extends to ~180 km from the river mouth (Laë et al. 2004), although peak discharge (~1500 m^3/s) in late September/October may result in fully riverine conditions as close as 80 km to the sea (Albaret et al. 2004). Between December and June, discharge may episodically cease completely (< 4.5 m^3/s), resulting in tidal effects and brackish water as far as 220 km upstream (Simier et al. 2006).

The Volta River, Ghana

The transboundary Volta River system enters the Gulf of Guinea via the common Volta estuary (5° 46′ 13″ N, 0° 40′ 41″ E) near Ada Foah, Ghana (Fig. 1b, c). Comprising ~400,000 km^2, its basin is drained by several larger rivers that originate from the plateau highlands of Burkina Faso. In north-central Ghana ~ 500 km north of the coastline, the Black and White Volta branches merge, before entering the Volta Lake together with the Oti River. The Volta Lake became one of the world's largest artificial reservoirs with the construction of the Akosombo dam in 1965 and two hydropower facilities at Akosombo and Kpong in 1982. The flow regime and sediment transport in the Lower Volta have been substantially altered by the dam and are now primarily governed by turbines, altogether reducing the natural discharge volume and effectively muting seasonal fluctuations (Logah et al. 2017; Ndehedehe et al. 2017). In response to the damming, the saline boundary has moved from previously ~40 to ~15 km from the river mouth today (Petr 1986). The climate is monsoonal and characteristic of the Southern Savannah zone with an average annual rainfall of ~ 870 mm, most of which occurs between March and November during the main wet season in May/June, and a second, less pronounced rainy period between September and November (Logah et al. 2017). The estuary includes various open and restricted lagoons, some of which developed following the dam constructions. The largest of these is the Keta Lagoon east of the river mouth (Fig. 1c), which is generally disconnected from the sea with the exception of seasonal seawater influx at high tides. Mangroves fringe the lower estuary, while grassland and shrub are dominant upstream (UNEP-GEF Volta Project 2013).

The Sine-Saloum, Senegal

The Sine-Saloum estuary (between 13° 40′ N and 14° 20′ N) encompasses ca. 800 km^2 of open water across a complex network of numerous interconnected smaller channels and creeks, and the three main branches Saloum,

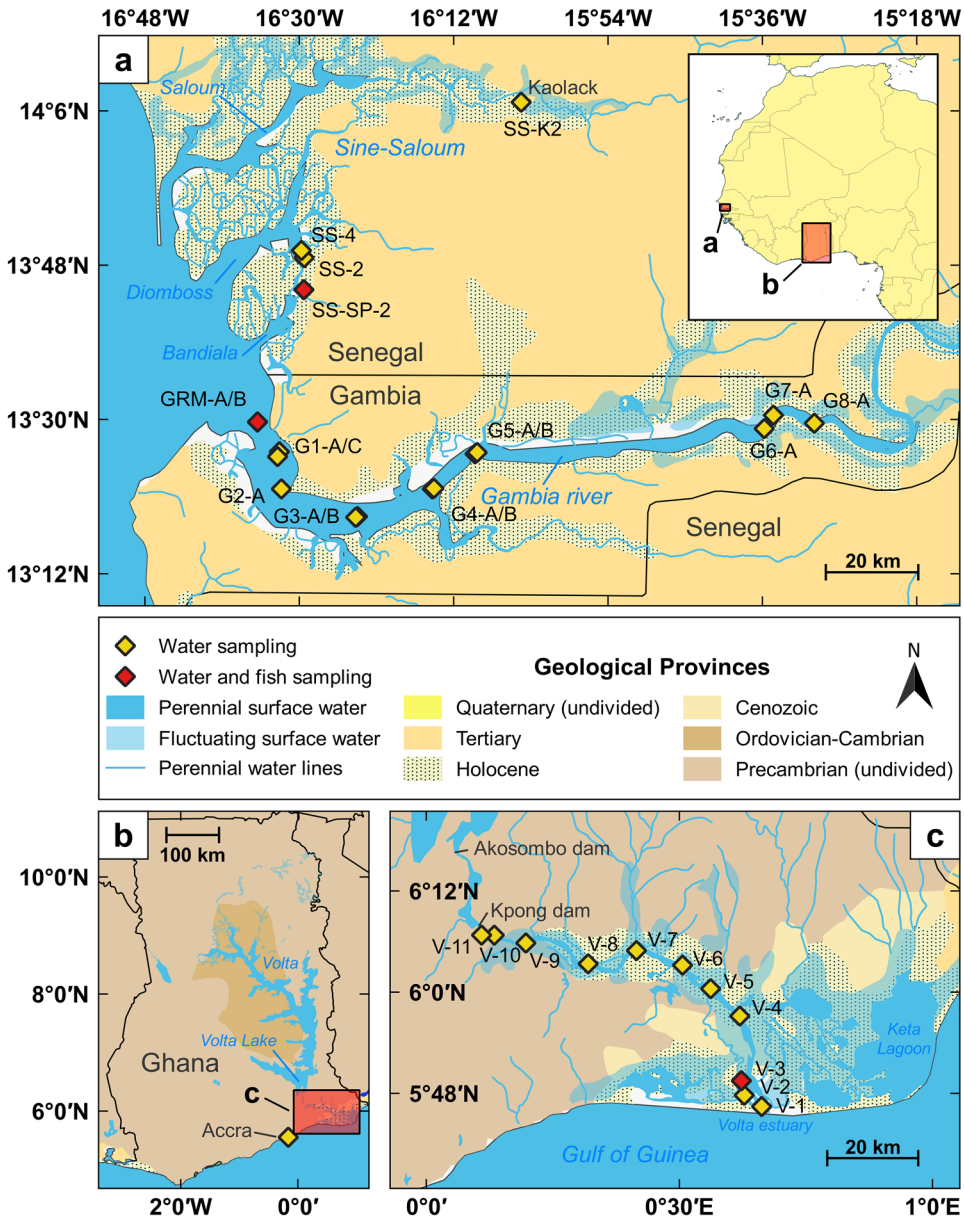

Fig. 1 Overview of sampling stations in the three estuaries in NW Africa. Locations of water samples are indicated as yellow diamonds with corresponding sample ID (A, B, and C denote replicates). Otoliths analysed in this study were retrieved from fish caught at stations marked with red diamonds. Perennial water bodies and connecting streams of water are indicated by solid blue areas and lines, respectively, while non-perennial (e.g., seasonally fluctuating) systems are marked by stippled blue areas. Close-up maps show the predominant surface lithology based on data and classifications from Persits et al. (2002). **a** The Sine-Saloum delta (Senegal) with its three main branches in the north, and the Gambia River (The Gambia) in the south. **b** Overview of the extensive Volta Basin in Ghana. The yellow diamond indicates the sample location at Accra beach. **c** Sample locations in the Volta River estuary from the river mouth to the Kpong dam. A more detailed overview of geological units of the Lower Volta can be found in Jørgensen and Banoeng-Yakubo (2001)

Diomboss, and Bandiala (Fig. 1a). Its southern extent is almost exclusively covered in mangrove forests, which progressively vanish towards the sparsely vegetated North (Simier et al. 2004). The ~29,700 km^2 large drainage basin has a Soudano-Sahelian climate, and freshwater input to the estuary is limited to local rainfall (~700 mm/year), most of which occurs during the wet season from July to October (Doumouya et al. 2016). In the course of the Sahelian droughts (1968–1993), a lack of rainfall, coinciding intense evaporation rates, deforestation and tidal seawater intrusions resulted in the inversion of the salinity gradient that generally persists throughout all seasons (Faye et al. 2019). As a consequence, salinities increase from the river mouth (~36) to over 100 in Kaolack, ~110 km upstream, while lower salinities are only rarely observed after the rainy season in the seaward part of the estuary. Regardless of the season, discharge is negligible and the estuary is tidally influenced (Azzoug et al. 2012; Mikhailov and Isupova 2008; Simier et al. 2004).

Methodology

Collection and Preparation of Water Samples

Sampling campaigns in the estuaries of the Sine-Saloum (Senegal), Volta River (Ghana) and Gambia River (The Gambia) were carried out in 2017 (see Fig. 1 and Table 1 for sampling locations and geochemical data of water samples). In the

hypersaline Sine-Saloum, water samples were obtained from 7 stations in the comparably narrow and shallow (< 10 m) Bandiala branch along a ~12 km transect in the southern part of the delta in April (8^{th}/9^{th}) 2017 (Fig. 1). In addition, water was retrieved near Kaolack, situated approximately 110 km upstream along the main channel with typically extreme salinities. In Ghana and The Gambia, sampling locations were pre-selected aiming for representative samples across a salinity gradient from the river mouth (~marine) to fully riverine (~freshwater) conditions upstream. Stations were chosen based on previous records of estuarine salinity variability reported for these rivers (Albaret et al. 2004; Nyekodzi et al. 2018), and with considerations of the sampling period and expected precipitation amounts. The sampling in the Volta estuary was carried out between the 24^{th} and 28^{th} of August 2017. Water samples were collected from 11 stations between the river mouth and the Kpong Dam ~90 km upstream. In addition, one sample was retrieved off the beach in Accra away from any significant runoff as a local reference for seawater. In the Gambia River estuary, samples were collected from the 20^{th} to 23^{rd} of September 2017 towards the end of the wet season. Water samples were taken from the river mouth to ~150 km upstream at 9 stations. All water samples were obtained from the sub-surface (~20 cm depth) near the centre of the stream in plastic vials. The vials were rinsed with sample water several times before retrieving ca. 25 ml of water. In situ measurements of water temperature were taken at stations in the Volta estuary, and both temperature and subsurface salinities were measured for sampling locations in the Sine-Saloum and the Gambia River.

Upon arrival at the laboratory, water samples were filtered using surfactant-free cellulose acetate membrane syringe

Table 1 Geochemical data and locations of water samples analysed herein

Site	Sample ID	Salinity	$^{87}Sr/^{86}Sr$	$^{87}Sr/^{86}Sr$ 2SE	Sr (mg/L)	Ca (mg/L)	Sr/Ca (mmol/mol)	Latitude	Longitude
Gambia River	GRM-A	36.0	0.70918	0.00001	6.44	364.51	8.08	N 13° 29′ 41.5212″	W 16° 34′ 52.9212″
	GRM-B	35.4	0.709183	0.000005	6.32	368.25	7.85	N 13° 29′ 41.9388″	W 16° 34′ 52.4388″
	G1-A	32.5	0.70919	0.000004	5.86	336.54	7.96	N 13° 26′ 13.9812″	W 16° 32′ 19.7988″
	G1-C	34.8	0.709197	0.000006	6.16	359.87	7.83	N 13° 25′ 40.0188″	W 16° 32′ 32.5788″
	G2-A	26.3	0.709193	0.000006	4.37	252.08	7.93	N 13° 21′ 53.8812″	W 16° 32′ 5.5788″
	G3-A	26.4	0.709194	0.000006	4.47	257.02	7.96	N 13° 18′ 40.7988″	W 16° 23′ 13.2″
	G3-B	26.4	0.709207	0.000006	4.39	253.41	7.92	N 13° 18′ 34.8012″	W 16° 23′ 25.8″
	G4-A	14.2	0.709268	0.000009	1.72	101.42	7.76	N 13° 21′ 53.3988″	W 16° 14′ 29.4″
	G4-B	15.2	0.709267	0.000005	1.98	116.30	7.79	N 13° 21′ 57.6″	W 16° 14′ 18.6″
	G5-A	5.0	0.709322	0.000004	1.07	63.25	7.76	N 13° 25′ 58.8″	W 16° 9′ 30.6″
	G5-B	5.0	0.70932	0.000005	1.05	64.38	7.46	N 13° 26′ 8.9988″	W 16° 9′ 16.2″
	G6-A	0.1	0.71154	0.000007	0.05	5.23	4.55	N 13° 28′ 55.8012″	W 15° 35′ 47.4″
	G7-A	0.1	0.711748	0.000014	0.05	4.95	4.53	N 13° 30′ 29.9988″	W 15° 34′ 43.2012″
	G8-A	0.1	0.712091	0.000006	0.04	4.57	4.40	N 13° 29′ 33.6012″	W 15° 29′ 57.0012″
Volta River	Accra	41.0	0.709166	0.000005	7.60	484.07	7.18	N 5° 33′ 7.6464″	W 0° 9′ 50.7384″
	V-1	8.9	0.709511	0.000006	0.76	44.18	7.82	N 5° 46′ 25.9212″	E 0° 39′ 45″
	V-2	3.6	0.712354	0.000012	0.08	6.29	5.82	N 5° 47′ 46.2012″	E 0° 37′ 40.7388″
	V-3	4.2	0.713336	0.000012	0.06	5.15	5.33	N 5° 49′ 29.46″	E 0° 37′ 20.5788″
	V-4	2.5	0.713449	0.000012	0.06	5.05	5.26	N 5° 57′ 9.9612″	E 0° 37′ 9.12″
	V-5	<0.0	0.713828	0.000014	0.05	4.87	4.70	N 6° 0′ 24.3″	E 0° 33′ 41.94″
	V-6	<0.0	0.713757	0.000008	0.06	5.20	5.19	N 6° 3′ 11.6388″	E 0° 30′ 21.8988″
	V-7	<0.0	0.713723	0.000016	0.06	4.93	5.20	N 6° 4′ 55.4988″	E 0° 24′ 54.4212″
	V-8	<0.0	0.713826	0.000015	0.05	5.03	4.64	N 6° 3′ 21.6″	E 0° 19′ 10.9812″
	V-9	<0.0	0.713932	0.00001	0.05	5.07	4.60	N 6° 5′ 49.6788″	E 0° 11′ 47.8788″
	V-10	<0.0	0.713922	0.000009	0.05	5.06	4.70	N 6° 6′ 45.18″	E 0° 8′ 3.48″
	V-11	<0.0	0.713919	0.000016	0.06	5.24	5.06	N 6° 6′ 45.7812″	E 0° 6′ 32.94″
Sine-Saloum	SS-K-2	100.0	0.709152	0.000008	22.19	1314.44	7.72	N 14° 7′ 0.59988″	W 16° 4′ 8.04″
	SS-SP-2	44.0	0.709147	0.000008	8.11	475.57	7.80	N 13° 45′ 8.39988″	W 16° 29′ 28.25988″
	SS-4	45.0	0.709179	0.000006	8.23	527.49	7.14	N 13° 49′ 42.6″	W 16° 29′ 45.35988″
	SS-2	43.9	0.709173	0.000005	8.42	495.86	7.77	N 13° 48′ 52.2″	W 16° 29′ 25.98″

filters (0.45 µm; Minisart®NML, Sartorius) to remove any particulate matter, as the dissolved strontium fraction was targeted. Although desirable, filtration in the field was not possible due to logistical constraints. However, on account of previous investigations we do not expect significant implications of delayed filtration in the context of this study (e.g., Palmer and Edmond 1989; Scaffidi et al. 2020). The filtrate was collected in acid-clean (10% HNO_3 bath) vials and was acidified to 2% (v/v) using HNO_3. Vials and filters were rinsed firstly with ultrapure water (Milli-Q®) and subsequently with sample prior to filtration. Separate aliquots of the acidified filtrate were taken for the determination of elemental concentrations and Sr isotopic compositions. Salinity of untreated aliquots was re-measured for each sample using a WTW®Multi 3410 multi-probe to provide comparable measurements between all locations. The instrument was operated using a non-linear temperature compensation and was calibrated prior to measurements to a KCl standard solution. Salinity measurements are reported as Practical Salinity (S_P; dimensionless).

Collection and Preparation of Catfish Otoliths

During respective sampling campaigns, Guinean sea catfish (*C. parkii*) were caught off the river bank in the Bandiala channel of the Sine-Saloum in close proximity of water sampling stations in the centre of the Gambia River mouth. In the Volta River, catch efforts yielded only the freshwater species *C. nigrodigitatus*, which were collected ~10 km from the river mouth on the river bank near sampling station V-3. All fish were caught by seine fishing with the aid of local fishermen (see Fig. 1 and Table 2 for catch information and otolith geochemical data). Immediately post-mortem we removed both lapillal otoliths (the largest type of otoliths in Ariid catfish) from the *C. parkii* and the two sagittal otoliths from the *C. nigrodigitatus*, cleaned the otoliths in tap water, and stored them in plastic vials after drying. Sagittae were selected for *C. nigrodigitatus* because of their clearer growth patterns relative to lapilli in this species (Fagade 1980). Sagittae and lapilli are both composed of aragonite and despite some demonstrated differences in chemical markers due to different growth patterns (Smith and Jones 2006), Sr isotope ratios are expected to equally reflect the ambient water composition due to the general lack of significant biological fractionation.

At the petrographic laboratory at the Leibniz Centre for Tropical Marine Research (ZMT), Bremen, Germany, fish otoliths were cleaned in an ultrasonic bath (Bandelin Sonorex) for 30 min, and dried at room temperature. From each estuary, otoliths from three female sub-adults were analysed. To avoid any potential differences in the elemental composition between the left and right otoliths as reported for some species (Gao et al. 2015; Loher et al. 2008), although found

Table 2 Otolith geochemical data and catch information of catfish used in this study. Ages for *C. parkii* were estimated based on the number of annuli, which were however not clearly distinguishable in all sections. Additional age estimates (in brackets) are based on age-length relationships using the Van Bertalanffy growth function and parameters established in Conand et al. (1995). Missing information is denoted by "n.a.". The fish were caught in April, August, and September 2017 in the Gambia River, Volta River, and Sine-Saloum, respectively

Site	Species	Sample ID	Total length (mm)	Forc length (mm)	Weight (g)	Age (years)	Sr/Ca (mmol/mol)	$^{87}Sr/^{86}Sr$	$^{87}Sr/^{86}Sr$ 2SE	Latitude	Longitude
Gambia River	*C. parkii*	RAP-GR-1	336	282	334	4.5 (3.3)	4.89	0.709213	0.000007	N 13° 29′ 43.1988″	W 16° 34′ 52.4388″
		RAP-GR-2	342	286	343	4.5 (3.4)	4.20	0.709203	0.000005	N 13° 29′ 43.1988″	W 16° 34′ 52.4388″
		RAP-GR-3	355	303	407	4.5 (3.7)	4.50	0.709227	0.000008	N 13° 29′ 43.1988″	W 16° 34′ 52.4388″
Volta River	*C. nigrodigitatus*	RCN-1	n.a	n.a	n.a	n.a	3.17	0.710750	0.000007	N 5° 49′ 29.46″	E 0° 37′ 20.5788″
		RCN-2	n.a	n.a	n.a	n.a	3.45	0.711875	0.000009	N 5° 49′ 29.46″	E 0° 37′ 20.5788″
		RCN-3	n.a	n.a	n.a	n.a	3.09	0.711446	0.000006	N 5° 49′ 29.46″	E 0° 37′ 20.5788″
Sine-Saloum	*C. parkii*	RAP-SS-1	400	353	647	5 (4.8)	4.72	0.709195	0.000005	N 13° 45′ 8.39988″	W 16° 29′ 28.25988″
		RAP-SS-2	408	355	573	5.5 (4.8)	4.71	0.709202	0.000007	N 13° 45′ 8.39988″	W 16° 29′ 28.25988″
		RAP-SS-3	395	342	541	5.5 (4.5)	4.25	0.709198	0.000007	N 13° 45′ 8.39988″	W 16° 29′ 28.25988″

to be negligible in others (Campana et al. 2000), the left otolith was consistently used. Otoliths of *C. parkii* specimens were cut in half through the core along the transversal plane with a Uniprec®Woko 50 high-precision saw using a 0.6 mm diamond coated blade. Posterior halves were embedded on glass slides with a two-component epoxy resin (Araldite®) and cut again transversally to produce sections of approximately 1 mm thickness. Section surfaces were further processed using a high-precision G&N®MPS2 surface grinder, and finally polished using a Logitech®PM2A instrument with a 1.0 and 0.25 µm diamond solution. This method enabled the identification of macrostructures, while allowing for potential future ontogenetic sub-sampling. In *C. parkii* otolith thin sections, couplets of translucent and opaque zones were counted as annual growth increments (annuli) between the opaque nucleus (primordial) and the otolith edge (time of death). This method yielded age estimates of ca. 4.5 and 5–5.5 years for fish from the Gambia River and Sine-Saloum, respectively. However, given that growth increments were not clearly distinguishable in all *C. parkii* otolith sections, we further estimated fish ages based on their fork lengths using the Von Bertalanffy growth function with published parameters for *C. parkii* (see Table 1 in Conand et al. 1995). Length-based estimates consistently yielded slightly younger ages of ca. 3.3 – 3.7 years (fork lengths of 282–303 mm) and 4.5–4.8 years (fork lengths of 342–355 mm) for the Gambia River and Sine-Saloum, respectively (Table 2). The anterior halves of the otoliths were crushed and homogenised using a ceramic grinder to produce bulk samples for geochemical analyses, i.e. skeletal material reflecting an integrated record of most of the individual's lifespan (excluding core material deposited during the earliest larval period). Most growth appears to coincide with the monsoonal period potentially due to higher food availability (Conand et al. 1995), and it is thus reasonable to assume that the bulk records are biased towards this season. Remaining parts of the posterior halves were archived. Necessitated by their small size, otoliths from *C. nigrodigitatus* individuals caught in the Volta River were prepared following a modified protocol. Accordingly, one sagittal otolith per *C. nigrodigitatus* specimen was crushed entirely in order to yield sufficient material for all analyses, while the second otolith was archived. This method and the lack of size information of the fish do not permit the estimation of fish ages. Images of prepared otolith samples are presented in Fig. 2.

Elemental Analysis

Element concentrations in otolith and water samples were measured using a Spectro CIROS Vision Inductively Coupled Plasma—Optical Emission Spectrometer (ICP-OES) at the ZMT. Sub-samples (~10 mg) of homogenised carbonate powder were dissolved in supra pure 0.5 molar HNO_3 (Carl Roth®). Depending on their salinity, aliquots of filtered and acidified water samples were diluted in 0.5 molar HNO_3 aiming for Ca concentrations of < 100 mg/L. Instrument calibration was achieved using commercial single-element standards. Each water and otolith sample was measured in triplicates bracketed by international reference standards JLs-1 (carbonate), SLRS-6 (water), and an in-house carbonate standard material (ZMT-CM1; coral aragonite) as consistency standard. Additional triplicate measurements of several water samples were completed at different dilutions for cross-validation, and the averages of different aliquot analyses are reported for these samples. The analytical accuracy for carbonate samples according to JLs-1 ($n=3$) was 3.3% for Sr (290.1 ± 16.1 mg/L) and 2.5% for Ca (403,488 ± 22,138 mg/L). The precision with respect to ZMT-CM1 ($n=2$) was 0.2% for Sr and 0.5% for Ca, respectively. For water samples, precision was 6.1% and 3.1% RSD for Sr (0.038 ± 0.001 mg/L) and Ca (0.013 ± 0.001 mg/L) according to SLRS-6 ($n=3$), respectively. Additional internal controls run alongside water and carbonate samples yielded both an accuracy and precision of better than 1.1% ($n=10$) for Sr and Ca.

Strontium Isotope Analysis

Strontium isotope ratios of water and otolith samples were determined by using a Thermo Scientific Triton Plus thermal ionisation mass spectrometer (TIMS) in the Isotope Geochemistry Laboratory at MARUM, University of Bremen, Germany. In preparation for the chemical isolation of Sr from undesired matrix elements, approximately 2 mg of homogenised carbonate powder derived from otolith samples were dissolved in 2 M HNO_3, dried, and redissolved in 500 µl of 2 M HNO_3. Water samples were prepared by evaporating aliquots of 0.2 to 7 ml, depending on the Sr concentration of each sample (aiming for ~ 200 ng of Sr in the resulting solids). Adapting the setup and procedure detailed in Deniel and Pin (2001), Sr was extracted using miniature columns loaded with 70 µl of Sr-spec ion exchange resin (Eichrom Technologies, LLC, USA). The collected Sr was loaded on single Re filaments with Ta-oxide emitter, and analysed by TIMS using a multi-dynamic acquisition routine. All $^{87}Sr/^{86}Sr$ measurements were normalised to a $^{86}Sr/^{88}Sr$ value of 0.11940 to correct for instrumental mass fractionation. The long-term external instrumental reproducibility according to NIST 987 standard material is $^{87}Sr/^{86}Sr$ 0.710249 ± 0.000014 (2σ, $n=263$) and is used in our calculations as a conservative estimate of the analytical uncertainty. This value is in excellent agreement with the average of published NIST 987 $^{87}Sr/^{86}Sr$ values (0.710249 ± 0.000066 (2σ), $n=1555$; values < 0.702 and > 0.703 were excluded, all data analysed by TIMS; source: http://georem.mpch-mainz.gwdg.de/, request February 2020).

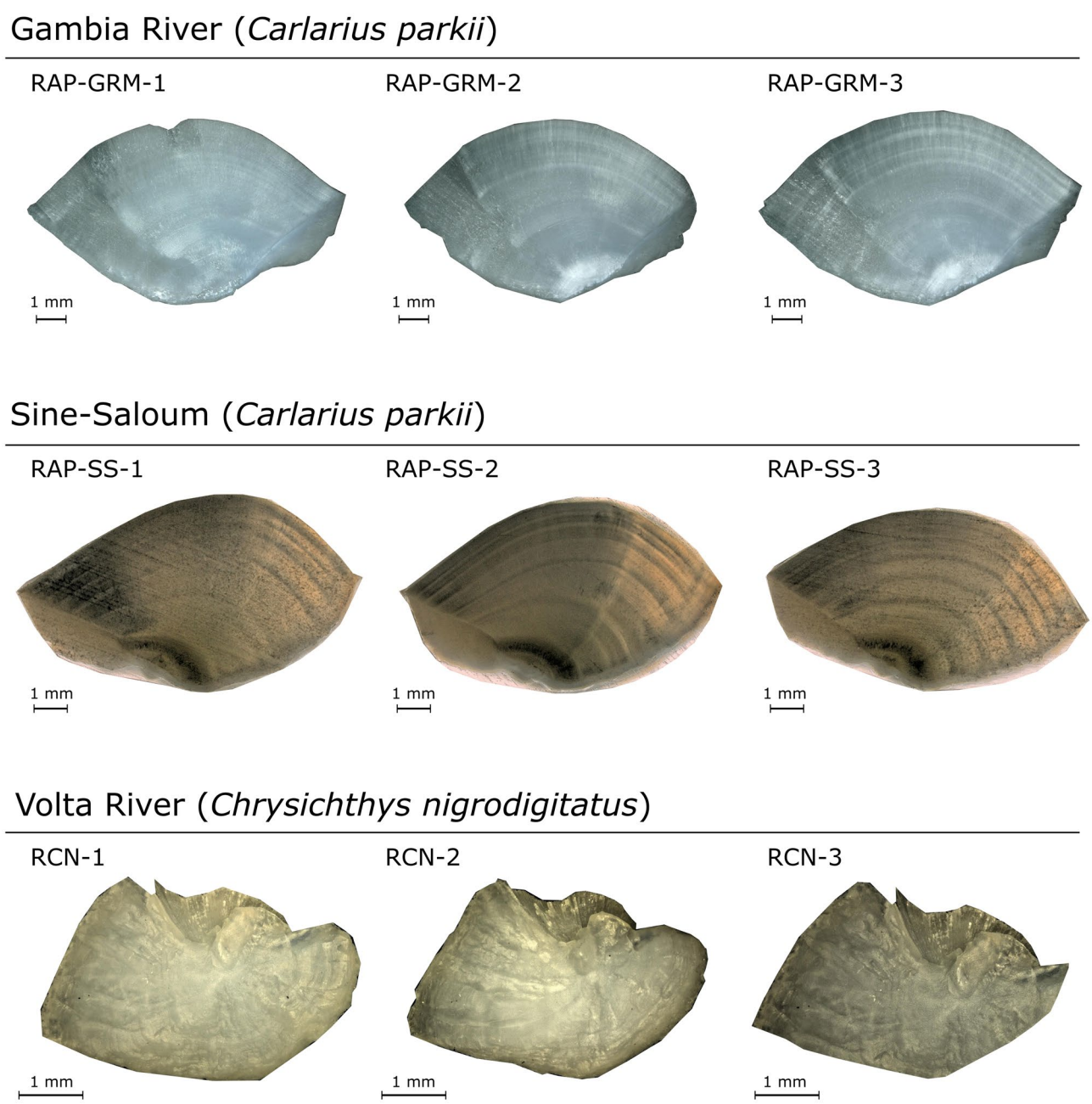

Fig. 2 Digital microscope images of catfish otolith samples. Note that different settings were required to visualise density bands in each sample, resulting in different colourations between *C. parkii* lapilli from the Sine-Saloum (thick sections) and the Gambia River (thin sections). In principle, paired dark and light growth bands are considered to represent one annual cycle, however, banding was not clearly distinguishable in all sections. *C. nigrodigitatus* sagittal otoliths were not sectioned due to their small size, and are shown here in whole

Mixing Models

To assess the systematics of Sr concentration and $^{87}Sr/^{86}Sr$ in water and carbonates along the estuarine salinity gradients, two-component mixing models were established for each study area. For a system with two end-members (e.g., seawater and freshwater) A and B with different concentrations of Sr and distinct $^{87}Sr/^{86}Sr$ values, a general mixing model in hyperbolic form can be described for the Sr isotopic composition of a mixture M between the two components as (Eq. 1):

$$\left(\frac{^{87}Sr}{^{86}Sr}\right)_M = \left(\frac{^{87}Sr}{^{86}Sr}\right)_A * f_A * \left(\frac{Sr_A}{Sr_M}\right) + \left(\frac{^{87}Sr}{^{86}Sr}\right)_B * (1 - f_A) * \left(\frac{Sr_B}{Sr_M}\right) \quad (1)$$

where Sr_A, Sr_B, and Sr_M are the Sr concentrations of components A and B, and a mixture M of the two, respectively. Ratios $(^{87}Sr/^{86}Sr)_A$, $(^{87}Sr/^{86}Sr)_B$, and $(^{87}Sr/^{86}Sr)_M$ represent the respective Sr isotopic compositions (Faure and Mensing 2005). The factor f_A denotes the fraction of component A in the mixture M, given as (Eq. 2):

$$f_A = \frac{A}{A+B} \tag{2}$$

As detailed in Wierzbowski (2013) and Phillis et al. (2011), Eq. (1) can be used to derive an expression that relates $^{87}Sr/^{86}Sr$ values of carbonate precipitates (e.g., otoliths or bivalve shells) to the salinity of their source water by redefining the mixing factor of Eq. (2) in terms of salinity (Eq. 3):

$$f_A = \frac{Salinity_M - Salinity_B}{Salinity_A - Salinity_B} \tag{3}$$

Elimination of f_A, rearrangement, and a revision of subscripts to denote the mixture as brackish water (subscript *bw*), end-members as freshwater (*fw*) and seawater (*sw*), and including the otolith chemical composition (subscript *carb*), finally yields (Eq. 4):

$$Salinity_{bw} = \frac{Salinity_{sw} * \left[(^{87}Sr/^{86}Sr)_{carb} * Sr_{fw} - (^{87}Sr/^{86}Sr)_{fw} * Sr_{fw}\right]}{\left[(^{87}Sr/^{86}Sr)_{sw} * Sr_{sw} - (^{87}Sr/^{86}Sr)_{fw} * Sr_{fw} - (^{87}Sr/^{86}Sr)_{carb} * (Sr_{sw} - Sr_{fw})\right]} \tag{4}$$

These Sr mixing models assume conservative properties (i.e. that Sr concentrations and $^{87}Sr/^{86}Sr$ are not altered by biological processes), and that mixing occurs between two distinct components with constant elemental and isotopic compositions (Faure 1986). The validity of these assumptions was evaluated by inspecting the nature and strength of various relationships between measured and derived chemical signatures of water samples, namely $^{87}Sr/^{86}Sr$, concentrations of Sr and Ca, the reciprocal of Sr concentrations (1/Sr), and salinity. Adapting the approach of Wierzbowski (2013), we considered a deviation from the marine end-member beyond external instrumental reproducibility as a means to compute the upper salinity threshold (herein termed the "salinity determination threshold") for identifying the effect of salinity on $^{87}Sr/^{86}Sr$. Above this limit, analytical uncertainty precludes reliable correlations between salinity and $^{87}Sr/^{86}Sr$.

Mixing models for the Gambia River, Volta River, and Sine-Saloum estuaries were established based on observed end-member Sr concentrations, $^{87}Sr/^{86}Sr$ measurements and salinities (Table 3). In the Gambia River and Volta River estuaries, freshwater end-members were determined using measured properties of samples taken furthest upstream. Analyses of water samples from the Gambia River mouth and Accra beach (Ghana) were considered as the marine end-member for respective models. Properties observed at Kaolack served as an upstream end-member for the Sine-Saloum, although it is noted that this station corresponds to the highest salinity due to the inverse estuarine gradient. The same marine end-member as for the Gambia River estuary was used, which is in close proximity to the Sine-Saloum delta. Empirical mixing lines and confidence intervals present the best curve fit determined using the Grapher® in-built statistics suite (Golden Software; Ver. 16.2) and solving for a hyperbolic regression model. The significance level was set to $\alpha = 0.05$ for all statistics.

Results

The Gambia River

A total of 14 water samples retrieved from the estuary of the Gambia River were analysed for $^{87}Sr/^{86}Sr$, along with Sr and Ca concentrations, and salinity. At large, all samples coherently reflected mixing along an estuarine gradient. $^{87}Sr/^{86}Sr$ of the water ranged from ~0.70918 (marine) at the river mouth to 0.71209 at the station furthest upstream. Over the approximately 150 km-long transect, salinities decreased from essentially marine values of 36.0 to a minimum of 0.1 in the upper estuary, while Sr concentrations showed a corresponding trend from 6.44 mg/L to 0.04 mg/L in samples with low salinities. $^{87}Sr/^{86}Sr$ of water were strongly positively correlated with the reciprocal of Sr concentrations ($R^2 > 0.99$, $p < 0.0001$, Fig. 3a), and showed an inverse linear relationship with Sr/Ca ($R = 0.99$, Fig. 3b). Sr concentrations were strongly correlated with Ca contents ($R > 0.99$, Fig. 3c), as well as with salinity ($R = 0.99$, Fig. 3d).

Table 3 Observed end-member compositions used in mixing models for the three estuaries. Note that salinities and Sr concentrations increase upstream in the Sine-Saloum

Location	End-member	Salinity	Sr (mg/L)	$^{87}Sr/^{86}Sr$
Gambia River	Seawater	36.0	6.44	0.70918
	Freshwater	0.1	0.04	0.71209
Volta River	Seawater	41.0	7.60	0.70917
	Freshwater	0.01	0.06	0.71392
Sine-Saloum	Seawater	36.0	6.44	0.70918
	Upstream	100	22.19	0.70915

Based on the observed end-members (Table 3), salinity and $^{87}Sr/^{86}Sr$ of water were related by a hyperbolic mixing model approaching an asymptote for salinities above ~15 (Fig. 4a). The relationship was most pronounced at salinities below 10, with a decrease in $^{87}Sr/^{86}Sr$ of > 0.00270 corresponding to a salinity increase from 0.1 to 5.0. For samples with salinities of 5 or higher (i.e. those for which the mixing line approaches an asymptote), a strong linear relationship between salinity and $^{87}Sr/^{86}Sr$ was observed ($R^2 = 0.94$, $p < 0.0001$, Fig. 4a inlet). However, samples with salinities of 25 or higher were indistinguishable based on their $^{87}Sr/^{86}Sr$ ratios considering the external reproducibility. There were clear differences between samples with salinities of ~5, ~15 and those with 25 or more. Based on a deviation from the marine end-member beyond instrumental reproducibility, the salinity determination threshold, or minimal measurable effect of salinity on $^{87}Sr/^{86}Sr$ as defined by Wierzbowski (2013), was calculated to be ~20. A similar although less pronounced hyperbolic relationship was observed between Sr/Ca measurements of water samples and salinity (Fig. 4b), with ratios increasing with salinity. The otolith Sr isotopic ratios of three *C. parkii* aged ca. 4 years (considering both methods for age determination) caught in the lower Gambia River estuary varied between 0.70920 and 0.70923, slightly more radiogenic (i.e. enriched in ^{87}Sr) than the seawater composition. Carbonate Sr/Ca values were between 4.20 and 4.89 mmol/mol. Based on Eq. (4) and the external instrumental reproducibility (± 0.000014), these values translate to an overall salinity range from 9 to 25. The smallest (~5) and largest (~12) ranges of Sr-based salinities estimates corresponded to the highest (0.70923) and lowest (0.70920) otolith $^{87}Sr/^{86}Sr$ values, respectively.

The Volta River

Salinities in the estuary of the Volta River reflected considerable freshwater discharge at the time of the sampling campaign, ranging from < 0.01 upstream to ~9 at the river mouth (Table 1). The shallow water at Accra beach had a salinity of 41 and a marine $^{87}Sr/^{86}Sr$ value of 0.70917. Estuarine samples varied in their Sr contents and isotopic compositions between 0.76 mg/L and 0.70951 at the location closest to seawater, and ~ 0.05 mg/L and 0.71393 near the Kpong dam. The last seven stations (from ~30 km from the river mouth) with salinities of < 0.1 yielded Sr contents consistently between 0.05 and 0.06 mg/L. $^{87}Sr/^{86}Sr$ of these samples continued to increase to a maximum of

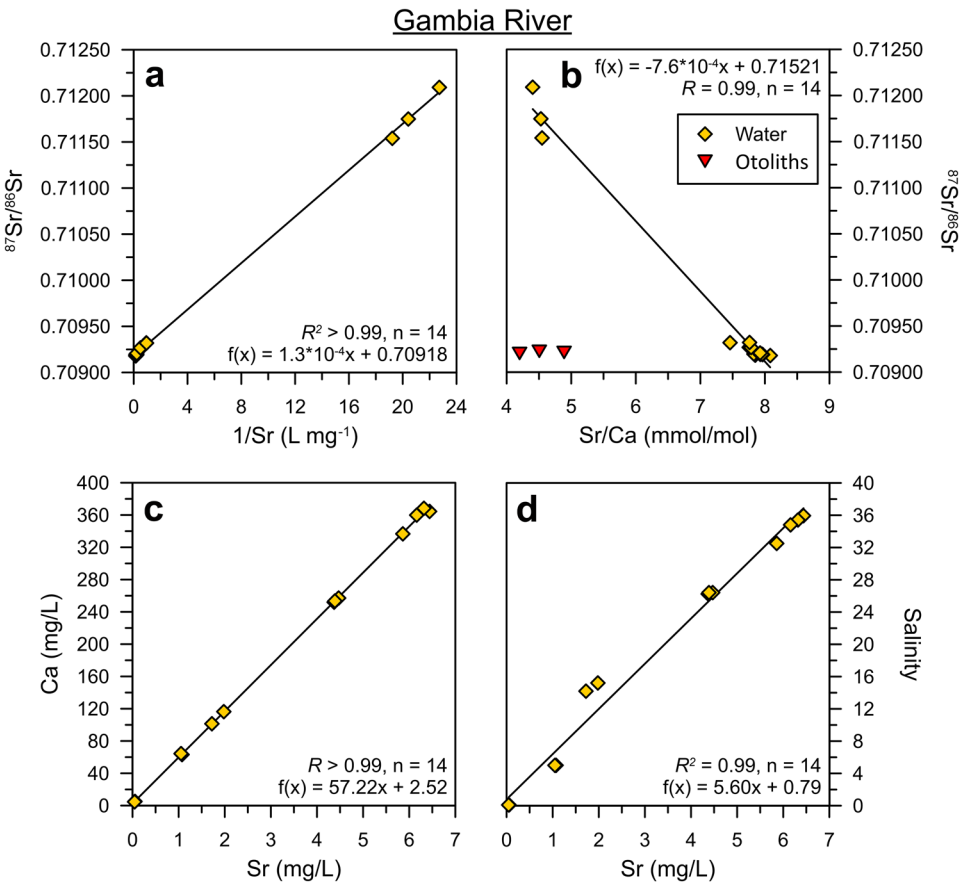

Fig. 3 Relationships between different geochemical signatures in water samples (yellow diamonds) and *C. parkii* otoliths (red triangles) from the estuary of the Gambia River. Analytical uncertainties are included in the symbol size. Equations and correlation coefficients for respective linear fits are presented in each plot. **a** Inverse Sr concentrations versus $^{87}Sr/^{86}Sr$ in water samples. **b** Sr/Ca versus $^{87}Sr/^{86}Sr$ in water samples and *C. parkii* otoliths. **c** Sr versus Ca concentrations. **d** Sr concentrations versus salinity

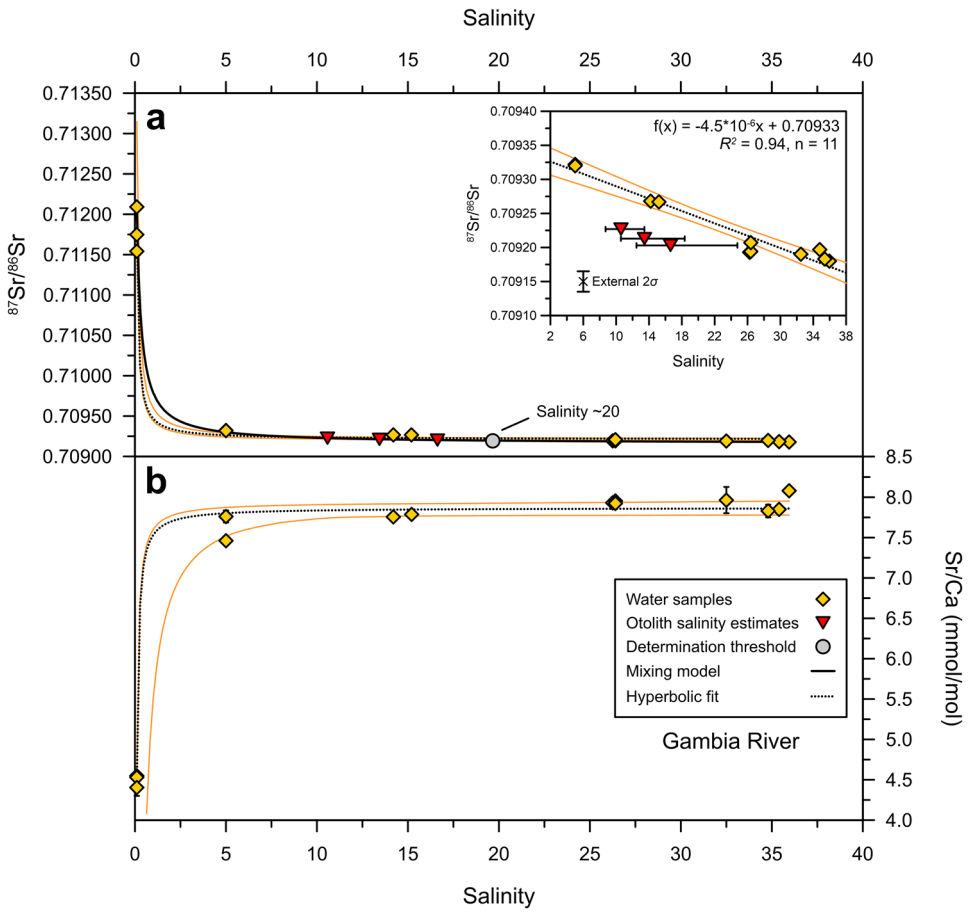

Fig. 4 Sr isotope ratios and Sr/Ca versus salinity in the Gambia River estuary. Water and *C. parkii* otoliths are shown as yellow diamonds and red triangles, respectively. **a** Mixing model of water $^{87}Sr/^{86}Sr$ across the salinity gradient (solid black line). End-member compositions used for the model are presented in Table 3. The inlet shows data that lie along the asymptote in the main graph (salinity ≥ 5), which are well described by a linear relationship ($R^2 = 0.94$, $p < 0.0001$; orange lines reflect 95% confidence intervals). The salinity determination threshold (grey circle) is based on a deviation of ≥ 0.000014 from the marine end-member (~0.70918) and estimated to be ~20. Salinities for bulk otolith samples were estimated based on their $^{87}Sr/^{86}Sr$ values and Eq. (4). Error bars of otolith salinity reconstructions shown in the inlet are calculated based on the external instrumental reproducibility of ± 0.000014 for $^{87}Sr/^{86}Sr$ with respect to NIST 987 standard material. These error bars are omitted in the main graph of **a** for clarity. Uncertainties of individual samples are smaller than the symbol size. **b** Sr/Ca versus salinity. Error bars for Sr/Ca present 1σ based on replicate measurements. The dotted black lines and solid orange lines indicate a hyperbolic best-fit curve and 95% confidence intervals computed for respective water samples in both **a** and **b**

0.71393 at station V-10. Water $^{87}Sr/^{86}Sr$ values were positively correlated with inverse Sr concentrations ($R^2 = 0.98$, $p < 0.0001$, Fig. 5a), and negatively correlated with Sr/Ca ($R = 0.97$, Fig. 5b). Freshwater samples were largely consistent amongst each other in both relationships, with samples from the lower estuary and river mouth showing a larger variability. Sr concentrations of samples from the Lower Volta (excluding the sample from Accra beach) were strongly correlated with Ca contents ($R > 0.99$, Fig. 5c), and to a lesser extent with salinity ($R = 0.84$, Fig. 5d). Water from Accra beach was not included in this correlation to avoid bias due to the substantial difference in Sr content and salinity compared to the estuarine samples.

The mixing model derived for the Volta estuary based on the observed freshwater end-member and the marine sample from Accra approached an asymptote from ~15, with a salinity determination threshold of ~29 (Fig. 6a). Sr/Ca measurements of water samples and salinity did not show a distinctive relationship (Fig. 6b). $^{87}Sr/^{86}Sr$ ratios of *C. nigrodigitatus* otoliths collected from the lower Volta estuary ranged from 0.71075 to 0.71188, with Sr/Ca values between 3.09 and 3.45 mmol/mol (Fig. 5b). Based on bulk otolith $^{87}Sr/^{86}Sr$ measurements, reconstructed salinities (Eq. 4) for the three individuals were consistently below 1 (0.2 to 0.6) with minimal ranges of each salinity estimate (< 0.1; Fig. 6a).

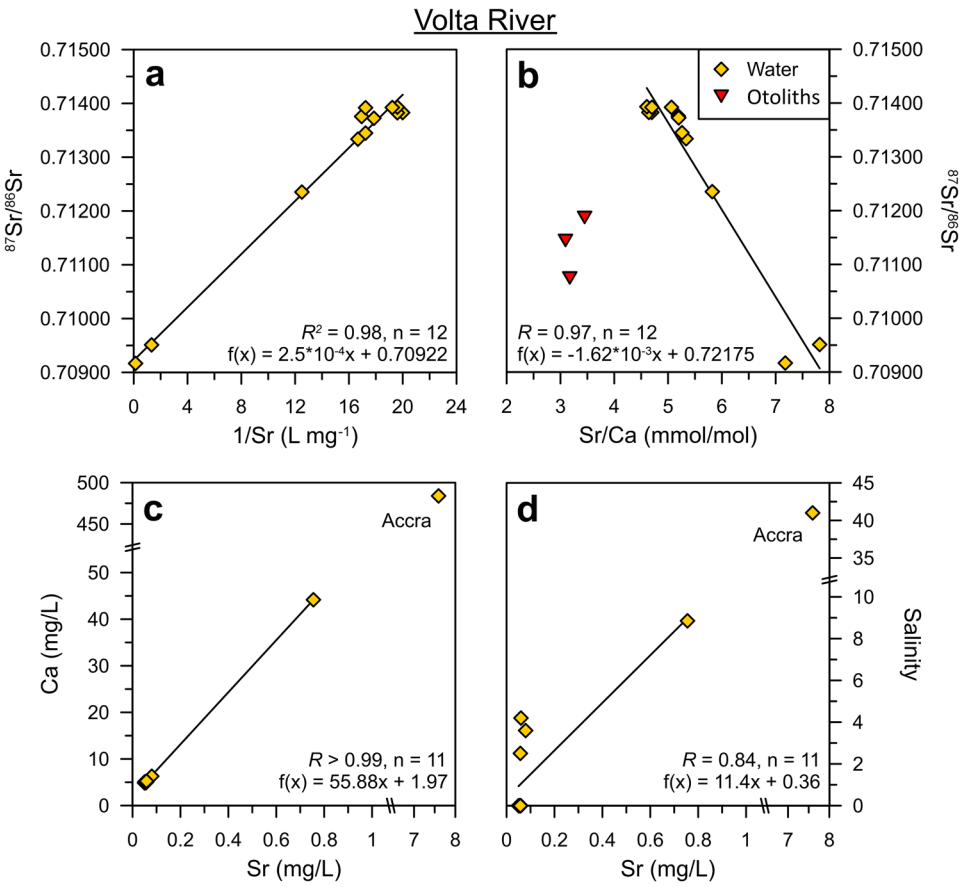

Fig. 5 Relationships between different geochemical signatures in water samples (yellow diamonds) and *C. nigrodigitatus* otoliths (red triangles) from the estuary of the Volta River. Analytical uncertainties are included in the symbol size. Equations and correlation coefficients for respective linear fits are presented in each plot. Note that plots **c** and **d** include axis breaks and omit the Accra sample in correlations as the lack of samples of intermediate salinity would bias the statistic. **a** Inverse Sr concentrations versus $^{87}Sr/^{86}Sr$ in water samples. **b** Sr/Ca versus $^{87}Sr/^{86}Sr$ in water samples and *C. nigrodigitatus* otoliths. **c** Sr versus Ca concentrations. **d** Sr concentrations versus salinity

The Sine-Saloum

The seven water samples retrieved from the Bandiala channel in the southern Sine-Saloum estuary did not exhibit a pronounced gradient in salinity across the sampled transect in the lower estuary, while two samples near Kaolack showed extreme salinities exceeding the instrumental limit of 100. Given the homogeneity in salinity and prospective redundancy for the study's objectives, three samples covering the observed range of 43.9 to 45.0 were prioritised for further analysis of elemental compositions and $^{87}Sr/^{86}Sr$, along with one sample from Kaolack (Table 1). Corresponding to the persistent salinities in the lower transect, Sr concentrations in water samples showed little variation with an average of 8.25 ± 0.16 mg/L (1σ) similar to seawater, and were exceptionally high at Kaolack (22.19 mg/L). There were no pronounced differences between the $^{87}Sr/^{86}Sr$ values of water from the estuarine stations and Kaolack at the external instrumental reproducibility, with all $^{87}Sr/^{86}Sr$ measurements varying between 0.70915 and the marine composition of 0.70918 (Fig. 7). Water samples were thereby on average less radiogenic than seawater, whereas otolith values of *C. parkii* (aged ca. 5 years) were consistently higher (~0.70920) than the marine signature. Sr/Ca ratios differed considerably between otoliths and water, varying from 4.25 to 4.72 mmol/mol and 7.14 to 7.80 mmol/mol, respectively. An adequate mixing model for the Sine-Saloum could not be established given the observed Sr signatures and salinities of assumed end-members (Table 3).

Discussion

The Sr systematics of water and fish otoliths along estuarine mixing zones have previously been assessed for a range of major river systems other than the ones studied here, providing valuable reference to disentangle the life-histories of several fish species of high ecological and economic significance (Brennan et al. 2015; Hobbs et al. 2019; Kennedy et al. 2002; Phillis et al. 2011). Quantitative relationships between $^{87}Sr/^{86}Sr$ and salinity of water across estuarine gradients can be derived for the mixture of different components when their respective geochemical compositions are known. However, these relationships vary depending on the sources of weathering products released to the water, and are linked to the rock types and sediments within the drainage area, as well as the local hydrology (Sessa et al. 2012). Accordingly, the three estuaries assessed in this study showed clear

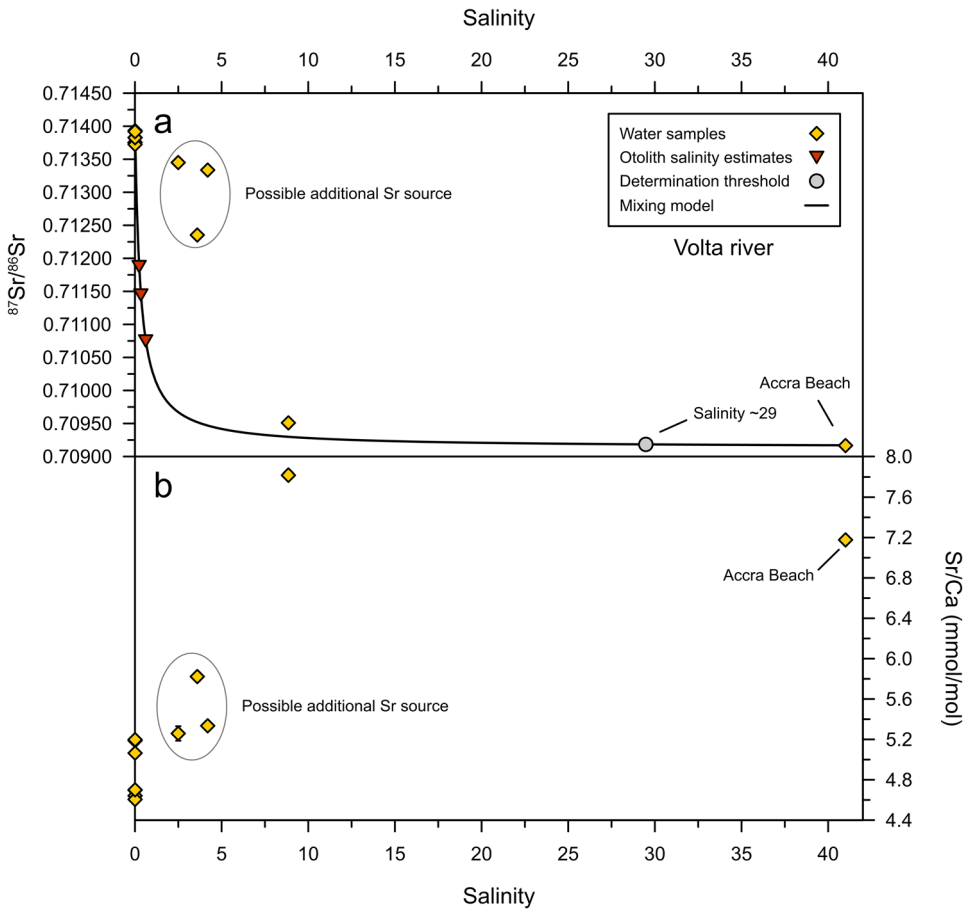

Fig. 6 Sr isotope ratios and Sr/Ca versus salinity in the Volta River estuary. Water and *C. nigrodigitatus* otoliths are shown as yellow diamonds and red triangles, respectively. **a** Mixing model of water $^{87}Sr/^{86}Sr$ across the salinity gradient (solid black line). End-member compositions used for the model are presented in Table 3. The salinity determination threshold (grey circle) is based on a deviation of ≥0.000014 from the marine end-member (~0.70918) and estimated to be ~29. Salinities for bulk otolith samples were estimated based on their $^{87}Sr/^{86}Sr$ signatures and Eq. 4. Otolith salinity ranges were calculated using the instrumental reproducibility of ±0.000014 for $^{87}Sr/^{86}Sr$ with respect to NIST 987 standard material. All uncertainties, including instrumental reproducibility are smaller than the symbol size. **b** Sr/Ca versus salinity. Error bars for Sr/Ca present 1σ based on replicate measurements. Empirical curve fitting did not yield an adequate hyperbolic relationship for the data in both **a** and **b** due to three samples (encircled) possibly representing an additional Sr source

differences in their Sr geochemistry and correlation of the latter with salinity, demonstrating both desirable criteria as well as limiting factors and sampling requirements for this approach.

The Gambia River

Of the three estuaries considered in this study, samples from the Gambia River exhibited the best agreement between theoretically and empirically determined relationships of $^{87}Sr/^{86}Sr$ and salinity in the estuarine mixing zone (Fig. 4a). These findings demonstrate the potential of $^{87}Sr/^{86}Sr$ measurements as quantitative proxy systems. The strong correlations of $^{87}Sr/^{86}Sr$ signatures of water with 1/Sr, as well as with Sr/Ca, provide good indications that the assumption of a two-component mixing system is largely valid (Fig. 3a, b). The available Sr is effectively added or removed by changes in the relative contribution of freshwater and seawater end-members (Capo et al. 1998; Holmden and Hudson 2003). This was supported by a pronounced linear relationship between Sr and Ca concentrations across the salinity gradient, likewise indicative of a binary mixture (Fig. 3c). The high correlation between Sr contents of water and salinity in turn indicates a conservative behaviour of Sr in the estuarine mixing zone (Fig. 3d), which is another critical prerequisite for derived models to apply (Faure 1986).

In line with these observations, the theoretical mixing line based on observed freshwater and seawater end-members (Table 3) was in very good agreement with water samples throughout the estuary (Fig. 4a), which are progressively

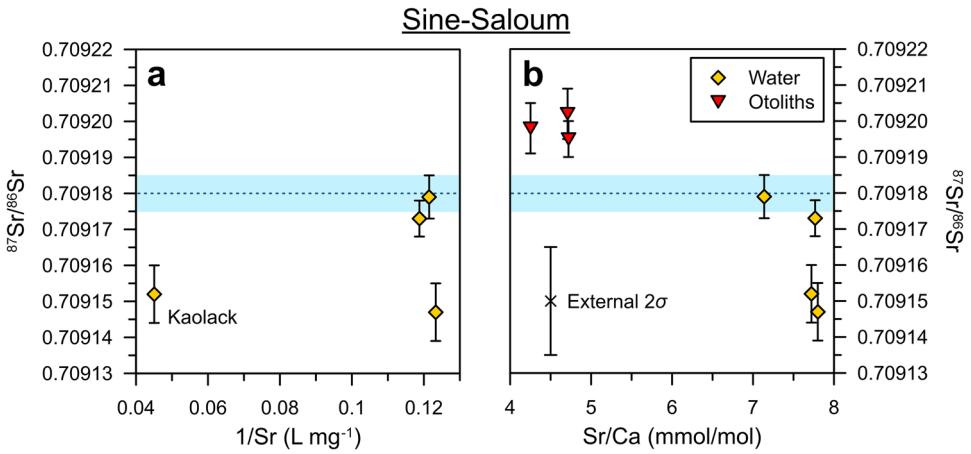

Fig. 7 Relationships between Sr isotopic signatures and elemental compositions of modern water (yellow diamonds) and *C. parkii* otoliths (red triangles) in the Sine-Saloum. The blue dotted lines and shadings indicate the average seawater value and corresponding 1σ (0.70918 ± 0.00001; Faure and Mensing 2005). Sample error bars indicate 2SE of the mean. The external instrumental reproducibility is given as 1σ according to NIST 987 ($n = 263$). **a** Inverse Sr concentrations versus $^{87}Sr/^{86}Sr$ in water samples from the lower Bandiala channel, and Kaolack (~110 km upstream). **b** Contrasting relationships of Sr/Ca versus $^{87}Sr/^{86}Sr$ between water samples and *C. parkii* otoliths

more radiogenic than seawater with distance to the river mouth. Accordingly, water from furthest upstream corresponded to the highest $^{87}Sr/^{86}Sr$ value of ~ 0.71209, and low Sr concentrations (~0.04 mg/L). Similarly, Sr/Ca and salinity measurements were well described by a hyperbolic relationship (Fig. 4a), comparable to those observed in studies using otolith Sr/Ca ratios as geochemical tracers (e.g., Nelson and Powers 2020; Phillis et al. 2011). Consistent with a known influence of various environmental factors on water and otolith Sr/Ca values, such as temperature (Gillanders 2005); however, the observed correlation between Sr/Ca and salinity is altogether less distinctive and arguably less predictable than that of $^{87}Sr/^{86}Sr$ with the latter (Fig. 4a). With respect to the magnitude of dissolved $^{87}Sr/^{86}Sr$ measurements, these values appear largely consistent with rock types and sediments in the drainage basin, although no specific regional accounts of Sr isotopic ratios of geological units or groundwater are available with the exception of larger-scale models (e.g., Peucker-Ehrenbrink and Fiske 2019). Most of the lower drainage region of the Gambia River is dominated by Quaternary clayey sands and sandstones that overlay the Cretaceous to Tertiary deposits of the Senegalese-Mauritanian sedimentary basin, while the upper watershed contains abundant Cambrian schists, quartzites, and crystalline rocks associated with the basement complex (Fig. 1; Meybeck et al. 1987; Whyte and Russell 1988). As part of the West African Craton, the basement mainly consists of crystalline magmatic and metamorphic rocks from the late Archean and early to mid-Proterozoic (~2.0 ga BP; Lécorché et al. 1991), the weathering products of which exhibit Sr isotopic signatures higher than those of seawater (Kumar et al. 2014). Previous investigations of the riverine water chemistry, although not including measurements of dissolved Sr, place the Gambia River in line with other rivers that show characteristic patterns in major ions for the predominant drainage of metamorphic and plutonic crystalline rocks, and/or sandstones and non-calcareous shales (Lesack et al. 1984; Meybeck et al. 1987). This entails generally rather low ionic contents, linked to high resistance of the dominant lithology to weathering, as well as the virtual absence of relief over the last approximately 500 km of the river course (Lesack et al. 1984). Although Cretaceous to Tertiary formations in the lower basin include limestones, Lesack et al. (1984) report an insignificant influence of carbonate weathering on the riverine geochemistry. Notwithstanding other controls on the solubility of Sr, the relatively low riverine Sr concentrations of ~ 0.04 mg/L observed in this study are in good agreement with the geological character of the catchment area. With respect to its geomorphology, the Gambia River is relatively simple without larger tributaries entering the main channel in the lower basin. Mixing in the estuary therefore appears to be effectively limited to a distinct seawater and freshwater component.

Consistent with observations from other rivers (e.g., Hobbs et al. 2010; Phillis et al. 2011; Reinhardt et al. 1998), $^{87}Sr/^{86}Sr$ was particularly sensitive to salinity variations at low salinities, below ~ 10–15. Since low salinity corresponds to low Sr concentrations (Fig. 3d), small variations in salinity go along with relatively large changes in the contribution of dissolved Sr from different components to the mixture. This in turn translates to large shifts of $^{87}Sr/^{86}Sr$ values. Reflected in the asymptotic character of the mixing curve in salinities of > 10, this effect becomes progressively less towards the river mouth (Fig. 4a). At higher salinities (and thus higher Sr concentrations), the addition or removal of

small amounts of Sr has comparably little impact on the overall $^{87}Sr/^{86}Sr$ value. The relationship between $^{87}Sr/^{86}Sr$ and salinity is therefore generally weaker at higher salinities, where $^{87}Sr/^{86}Sr$ ratios are less sensitive to changes in the dissolved Sr load (Ingram and Sloan 1992). This tendency is amplified in systems with particularly steep mixing curves, for instance in the highly radiogenic systems of northern Australia investigated by Crook et al. (2016), where estuarine mixing has little effect on $^{87}Sr/^{86}Sr$ above salinities of ~5. In consequence, quantitative mixing relationships between $^{87}Sr/^{86}Sr$ and salinity are most applicable to brackish waters with a considerable contribution of a freshwater end-member, but are ultimately limited by instrumental reproducibility (Wierzbowski 2013).

In the example of the Gambia River estuary, the salinity determination threshold was estimated at around 20 (Fig. 4a), based on a minimal deviation from the seawater end-member (0.70918) by 0.000014 (c.f., Reinhardt et al. 1998; Wierzbowski 2013). Accordingly, waters with salinities below 20 are expected to have a $^{87}Sr/^{86}Sr$ value significantly different to that of seawater. Despite a strong linear correlation of $^{87}Sr/^{86}Sr$ and salinity for salinities above 5 (Fig. 4a inlet), the resolvable range of salinity based on $^{87}Sr/^{86}Sr$ is in practice likely lower. This is suggested by the highly similar $^{87}Sr/^{86}Sr$ values in water with salinities of ~26 and 36 (Fig. 4a inlet) that would disallow a differentiation if preserved in biogenic carbonate structures, such as fish otoliths. This sensitivity constraint was exemplified by proxy salinities estimated from otolith $^{87}Sr/^{86}Sr$ measurements (± the external instrumental reproducibility) of sub-adult *C. parkii* caught in the river mouth, which translated into a considerable range in salinity from ~9 to 25. Corresponding to the higher sensitivity of $^{87}Sr/^{86}Sr$ to salinity changes at low salinities, the ranges in otolith-based salinities were larger for $^{87}Sr/^{86}Sr$ values closer to the seawater composition. The $^{87}Sr/^{86}Sr$ range can be expected to progressively decrease upstream to allow for more precise reconstructions of salinity (Widerlund and Andersson 2006). For the scope of this study, otolith geochemical analyses were limited to single bulk measurements, producing discrete values that represent a signal integrated over most of the individuals' life histories (~4 years for fish caught in the Gambia River). An assessment of the accuracy of predicted values compared to measured salinities was therefore not possible due to the lack of temporal resolution in the skeletal material, which can be achieved with sub-sampling techniques, such as microdrilling or laser ablation of otolith sections (e.g., Brennan et al. 2015; Hobbs et al. 2019; Kennedy et al. 2002). Regardless, the range in reconstructed salinities between the three individuals parallel the observations that *C. parkii* move across salinity gradients without obvious habitat preference once spawned (Simier et al. 2021).

In part due to socio-political reasons, land-use changes and modifications of the natural channel are to date limited in the Gambia River, making it a rare modern example of a West African river system close to its natural state (Sarré et al. 2018; Simier et al. 2006). Often considered a reference system for other NW African estuaries (Albaret et al. 2004; Louca et al. 2009; Simier et al. 2006), it thus presents a valuable opportunity for geochemical investigations and the study of migration patterns and life-histories of critical species. The good agreement between data and the derived mixing line show promising conditions for the use of temporally resolved otolith $^{87}Sr/^{86}Sr$ measurements and additional geochemical tracers to delineate preferred habitats of individuals during different life-stages via temporally-resolved analyses of otolith thin sections.

The Volta River

Similar to the Gambia River estuary, $^{87}Sr/^{86}Sr$ ratios of the Volta River estuary were inversely related to salinity, but were generally less consistent (Fig. 6a). In consequence, a mixing line derived from the compositions observed at Accra beach and near the Kpong dam upstream did not provide an accurate estimate for all samples, with three samples deviating considerably from the expected $^{87}Sr/^{86}Sr$ and salinity values (Fig. 6a). Empirical curve fitting did not yield an adequate hyperbolic relationship to describe these data, or to quantify a relation between Sr/Ca and salinity (Fig. 6b).

The limited predictability of $^{87}Sr/^{86}Sr$ and salinity was to an extent signified by the relationships amongst water parameters shown in Fig. 5, particularly that of Sr concentrations versus salinity with three samples clearly deviating from the trend (Fig. 5d). The apparent strong linear correlations between Sr and Ca concentrations ($R^2 > 0.99$, Fig. 5c) should be regarded with care given the lack of representative samples along the estuarine gradient between relatively fresh water (Sr contents < 1 mg/L) and seawater collected at Accra beach (7.60 mg/L). Under the assumption of a two-component system, the derived models are entirely based on the properties of two distinct end-members (i.e. seawater and freshwater). Data of samples presumably reflecting a mixture of these end-members therefore do not constitute to the shape of the mixing line. Given that multiple samples near the Kpong dam exhibit essentially identical Sr contents and isotopic ratios to the assigned freshwater end-member, the deviations between measured and calculated $^{87}Sr/^{86}Sr$ to salinity values are not readily explained by uncertainties related to the end-member compositions. Comparable deviations from linearity in mixing relationships (Fig. 5) observed in other estuaries and marginal seas have previously been attributed to submarine groundwater discharge (SGD; e.g., Huang et al. 2011; Rahaman and Singh 2012; Walther and

Niems 2015). SGD may significantly contribute to local Sr budgets and has the potential to alter estuarine $^{87}Sr/^{86}Sr$ values without notable concurrent changes in Sr concentrations (Rahaman and Singh 2012). In the Volta River, water samples collected at salinities between ca. 3 and 10 were consistently more radiogenic than the mixing line (Fig. 6a), whereas Sr concentrations were lower than conservative mixing would predict (Fig. 5d). These patterns are consistent with the expected chemistry of groundwater originating from the metamorphic lithology that would produce higher isotopic ratios than seawater. Exchange between shallow coastal groundwater aquifers of the Keta Basin and the estuary has been observed (Jørgensen and Banoeng-Yakubo 2001). It is thus likely that in absence of obvious tributaries (e.g., stream inlets or sewage) to the main channel, admixing of dissolved Sr from sub-surface contributions or poor vertical mixing contributed to the observed discrepancies.

Notwithstanding the uncertainty regarding the model validity, otolith-based salinity reconstructions of *C. nigrodigitatus* (caught at ~4) provide an example of the $^{87}Sr/^{86}Sr$—salinity proxy at low salinities. $^{87}Sr/^{86}Sr$ of all individuals consistently indicated values between ~0.2 and 0.6, with negligible ranges based on instrumental reproducibility of $^{87}Sr/^{86}Sr$. These salinity estimates are highly consistent with the habitat use of this species, which is understood to predominantly inhabit freshwater, and only temporarily enter brackish zones (Okyere and Boahemaa-Kobil 2020). Sr isotopic values integrated over the entire life of the fish (as reflected by the bulk measurements) are thus expected to be very close to the freshwater end-member composition. Although these reconstructed salinities clearly exceed realistic proxy accuracies, they illustrate the high predictability of salinity using carbonate $^{87}Sr/^{86}Sr$ values in freshwater-dominated environments, such as the upper estuarine mixing zone, or lagoon systems (Reinhardt et al. 1998; Wierzbowski 2013). For salinities below 10, for instance, Widerlund and Andersson (2006) report an accuracy better than ± 5% for $^{87}Sr/^{86}Sr$-based salinity reconstructions using bivalve shells in comparison to instrumental records. In the specific example of the Volta River, the exceptionally low range of reconstructed salinities can be attributed to the relatively steep mixing curve, the shape of which is in turn the result of analogously low Sr contents and high $^{87}Sr/^{86}Sr$ values of the freshwater end-member (see Phillis et al. (2011) for a schematic overview of mixing lines with different end-member constellations).

Information on the Sr isotopic composition of surface waters have so far been documented for few locations in the lower Volta estuary and the adjacent Keta Lagoon, in addition to a larger number of measurements from different groundwater aquifers in the Keta Basin (Jørgensen and Banoeng-Yakubo 2001). Surface water samples of Jørgensen and Banoeng-Yakubo (2001) were collected in the lower estuary and near the river mouth (~ seawater), as well as near Sogakope (~20 km from the sea), which were very well correlated in coordinates of 1/Sr and $^{87}Sr/^{86}Sr$ (Fig. 8). Between these samples and those from this study collected in close proximity, clear differences are evident. In particular, Sr contents (~0.20 mg/L) and $^{87}Sr/^{86}Sr$ (~0.711001) reported for the lower estuary near Ada Foah are considerably higher and lower, respectively, than those observed at essentially the same location (sample V-4, Fig. 8; 0.06 mg/L Sr, 0.713449). Observed discrepancies are likely due to temporal differences in discharge and a resulting spatial shift in the mixing zone, despite the heavily reduced temporal variability in flow in the Volta River since the construction of the dams (Ndehedehe et al. 2017). Regardless of this, some variations in the flow regimes remain, given that samples for this study were taken at the end of the wet season of 2017, whereas those of Jørgensen and Banoeng-Yakubo (2001) were retrieved over two periods in 1996 (wet season) and 1998 (end of dry season). The $^{87}Sr/^{86}Sr$ values of upstream samples from Sogakope are in good agreement with freshwater end-members observed in this study. The lithology of the upper estuary is dominated by metamorphic rocks, particularly gneiss, associated with the Dahomeyan formation of the Precambrian Man Shield that forms part of the West African Craton, whereas Quaternary coastal marine sands and gravel are found in the lower estuary and lagoons (Fig. 1). Deep groundwater from weathered Dahomeyan gneiss shows $^{87}Sr/^{86}Sr$ values in the range of 0.71299 to 0.71401 (Jørgensen and Banoeng-Yakubo 2001), which are highly coherent with those measured in water samples from near the Kpong dam (~0.71392), and thus are likely to represent the primary source of dissolved Sr to the upper estuary. Considering the age of the formations, and the large presence of K-bearing phases, such as biotite, Sr released during weathering can be assumed to exhibit rather radiogenic signatures in line with those observed in water (Bataille et al. 2012). The consistently low Sr concentrations (< 0.1 mg/L) may in turn be linked to the absence of major carbonates in the drainage area of the upper Volta estuary, and possibly poor mixing of the water column following heavy rainfall over the sampling period (I. Nuworkpor, personal communication). However, in light of the observed temporal and spatial variability, further sampling would be necessary to allow for reliable applications of mixing relationships for ecological studies.

The Sine-Saloum

The field campaign in the Sine-Saloum delta yielded water samples from the southern Bandiala branch and the main Saloum channel near Kaolack, approximately 110 km upstream. Although the low number and spatial coverage of samples due to logistical constraints naturally limit their

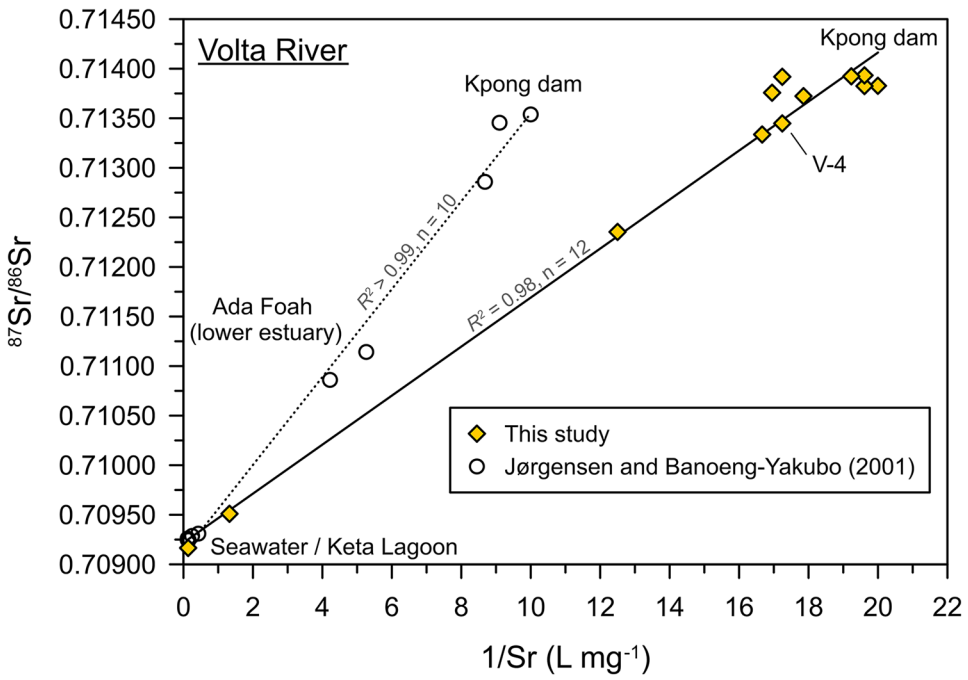

Fig. 8 Relationships between reciprocal Sr concentrations and $^{87}Sr/^{86}Sr$ in Volta River surface water samples from this study (yellow diamonds) in comparison to those from Jørgensen and Banoeng-Yakubo (2001) (circles). Solid and dotted lines indicate respective regression lines (both $p < 0.0001$). Note the discrepancies in Sr contents and $^{87}Sr/^{86}Sr$ between samples obtained from comparable locations within the estuary

informative value, these samples clearly depict the inverse hypersaline state of the system. Samples from the Bandiala branch were coherently more saline than seawater (~43), while salinities at Kaolack were extreme (> 100). Sr concentrations were exceptionally high in water from Kaolack, with contents nearly three times those typical for seawater. The $^{87}Sr/^{86}Sr$ measurements, however, did not show any systematic variations and correlation with Sr contents (Fig. 7), nor was any distinct relationship evident between Sr/Ca, $^{87}Sr/^{86}Sr$, or salinity.

Moreover, while $^{87}Sr/^{86}Sr$ ratios of water were on average slightly lower than the marine composition, the otoliths of three *C. parkii* individuals, all retrieved along the same transect as water samples, depicted consistently higher $^{87}Sr/^{86}Sr$ values. These data therefore contradict the assumption that Sr isotope ratios in catfish otoliths would reflect a mixture of Sr sourced from seawater and another component representing the Sine-Saloum.

The observed patterns and discrepancies between aqueous Sr content and isotopic ratios are linked to the present-day hydrological properties of the Sine-Saloum. Following the prolonged droughts in the 1970s in the Sahel zone, intense evaporation and tidal seawater intrusion resulted in the reversal of the formerly 'normal' estuary. At present, the inverse state is essentially modulated by the persistent high evaporation, deforestation (Faye et al. 2019), and low discharge and runoff (Descroix et al. 2020), despite a potential recovery of rainfall amount in the recent decade (Descroix et al. 2020; Faye et al. 2020). Regardless of $^{87}Sr/^{86}Sr$ measurements, the anomalous Sr and salinity regimes observed in the Sine-Saloum prohibit the establishment of a two-component mixing model due to non-conservative behaviour of Sr and salinity in the mixing zone, as similarly observed in the Coroong Lagoon of South Australia (Shao et al. 2021). In the Sine-Saloum and other arid systems (e.g., the Avon and Murchinson in Western Australia; Goldstein and Jacobsen 1987), this assumption is violated as excessive evaporation exerts an additional, external control on Sr concentrations and salinity, and their variations are consequently not solely due to mixing (De Villiers 2005; Flecker et al. 2002). It is perceivable that this limitation to the approach is inherent to inverse estuaries, considering that these generally form when evaporation greatly exceeds freshwater supply. Accordingly, the establishment of a two-component mixing model in estuaries subject to episodic dry spells (e.g., in semi-arid regions) may be similarly compromised, while information of interannual salinity and discharge variability may provide a means to evaluate this precondition.

With regards to the magnitude of $^{87}Sr/^{86}Sr$ values in waters from the Sine-Saloum, a strong influence of seawater throughout the estuary is noticeable, facilitated by the lack of any significant discharge (Mikhailov and Isupova 2008). The tendency of all water samples towards lower $^{87}Sr/^{86}Sr$ ratios than seawater is interesting given that the surficial lithology predominantly consists of Quaternary sands and alluvial deposits as part of the Senegalese-Mauritanian sedimentary basin (Fig. 1; Conrad and Lappartient 1987). Considering the observations from the nearby Gambia River, higher $^{87}Sr/^{86}Sr$ are generally expected. However, Faye et al. (2010) noted that groundwater from the underlying carbonate-bearing Continental Terminal aquifer (sediments of Cenozoic detrital marine origin) discharges to the

Bandiala branch of the Sine-Saloum where samples from this study were retrieved. SGD thus presents a potential source of Sr with lower $^{87}Sr/^{86}Sr$ ratios. Regardless of factors determining Sr concentrations of water in the delta, the isotopic compositions are expected to be reflected in otoliths of fish inhabiting the area (Sessa et al. 2012). Their elevated $^{87}Sr/^{86}Sr$ ratios are thus neither in line with any signatures observed within the Sine-Saloum, nor with those of a purely marine Sr source. This discrepancy may be explained by the proximity of the Sine-Saloum to the Gambia River mouth characterised by more radiogenic discharge, implying considerable migration of *C. parkii* between the two adjoining ecosystems. While several catch and modelling studies have assessed fish assemblages (e.g., Albaret et al. 2004; Brochier et al. 2013; Louca et al. 2009; Simier et al. 2004, 2006; Sloterdijk et al. 2017) and more specifically catfish populations (Diop et al. 2017; Simier et al. 2021) in these estuaries, the extent of migration between the Gambia and Sine-Saloum remains unclear in absence of tagging or tracing studies. Recent efforts to comprehensively assess the biology of West African sea catfish suggest a salinity range for *C. parkii* of 7 to 50, with highest fish numbers recorded at salinities of 15–20 and 30–35 (Simier et al. 2021). However, *C. parkii* clearly make wide use of the estuarine zone throughout all life-stages bar spawning (at sea), which is manifest in their frequent landings as far as 187 km upstream in the Gambia River (Laë et al. 2004). In the Sine-Saloum, extreme salinities typically restrict their presence to up to ca. 30 km from the sea (Panfili et al. 2006). Given that the two estuaries have Sr isotopic profiles sufficiently distinct from each other and the sea (although not systematic in the Sine-Saloum), we suggest that temporally-resolved otolith $^{87}Sr/^{86}Sr$ and elemental records could be used to complement catch datasets to help unravel population dynamics and constrain the degree of interconnectivity between the two estuaries. Moreover, while the modern hydrology impedes explicit correlations between salinity and the Sr isotopic composition in the Sine-Saloum, we emphasise the potential of utilising otolith or bivalve records from the abundant Holocene shell midden deposits found throughout the delta. Dating back from the modern to at least 5000 years BP (Hardy et al. 2016), these deposits are expected to provide unique insights into historic Sine-Saloum hydrology, and importantly, contribute information on the Holocene NW African climate evolution.

NW African Estuaries in the Global Context

The observed end-member $^{87}Sr/^{86}Sr$ signatures of all three NW African estuaries assessed in this study fall in the vicinity of the recently refined globally-weighted (by flux) estimate of continental runoff of ~0.71106 (Fig. 9; estimated by Peucker-Ehrenbrink and Fiske 2019), and are similar to those predicted for rivers in The Gambia and Senegal (~0.7100) in Beck et al. (2013). Considering the large range of $^{87}Sr/^{86}Sr$ values in rivers around the world, these systems are relatively similar in this regard but show more pronounced differences in Sr concentrations. With Sr concentrations of ~0.04 and 0.06 mg/L upstream, respectively, the Gambia River and Volta River plot in the lower range of rivers globally based on a compilation of comparable datasets (Fig. 9, data presented in Table S1), out of which the Marrakai Creek in northern Australia exhibits the most radiogenic (0.77785) Sr isotopic signatures with coincidingly lowest concentrations (ca. 0.002 mg/L Sr; Crook et al. 2015). Our findings confirm estimates of Sr concentrations modelled for large-scale drainage areas compiled by Peucker-Ehrenbrink and Fiske (2019), suggesting Western African catchments to have the lowest annual average Sr contents globally with regional minimum values of ~ 0.015 mg/L and generally limited continental runoff. On the other hand, our measurements suggest that the approximated Sr concentration (~0.26 mg/L) for rivers in The Gambia and Senegal as assumed for the global model of submarine groundwater discharge presented in Beck et al. (2013) presumably overestimates Sr inputs from these catchments.

An additional consideration regarding the Sr concentrations (and $^{87}Sr/^{86}Sr$ to a lesser extent) is the fact that the vast majority of studies (including this work) are limited to temporally and/or spatially discrete sampling efforts that inevitably cause bias. For instance, given the timing of sampling for this study in the late wet season, it is perceivable that relatively high freshwater discharge contributes to the low Sr contents observed, especially in the Volta River. Accordingly, replicate measurements at different times of the year with a high spatial coverage are recommended to account for discharge variability and better constrain estuarine $^{87}Sr/^{86}Sr$–salinity profiles (Crook et al. 2016). For example, Santos et al. (2014) observed considerable seasonal differences in mixing curves of multiple Amazonian rivers, whereas the Sr geochemistry of several estuaries along the coast of southern Texas presented in Walther and Niems (2015) proved highly consistent between years. Relative to its noticeably high Sr concentrations (~22 mg/L upstream) corresponding to high salinity, the $^{87}Sr/^{86}Sr$ value of water from the Sine-Saloum was notably low, and similar to seawater. This stands in contrast to other arid, evaporation-dominated basins, such as the Avon (albeit not directly connected to the sea) and Murchinson rivers in Western Australia. These systems likewise have rather high Sr concentrations due to low discharge and consequently prolonged time for the mobilisation of ions (Modestou et al. 2017), but analogously higher $^{87}Sr/^{86}Sr$ values without a clear link to their catchment geology (Fig. 9; Goldstein and Jacobsen 1987; Veizer et al. 1999). In terms of its isotopic composition, the upstream end-member of the Sine-Saloum is thereby

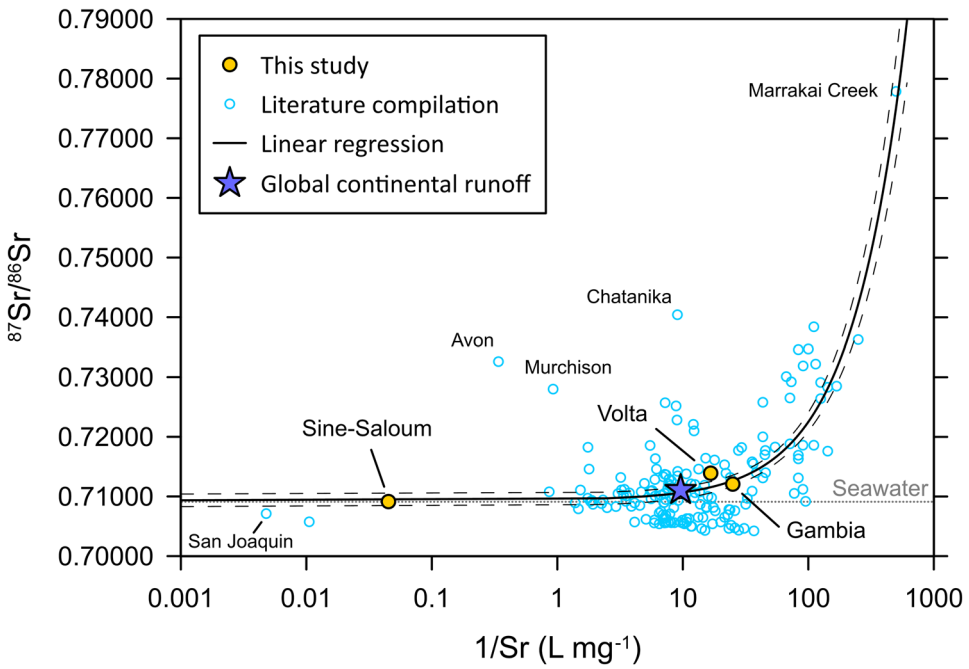

Fig. 9 $^{87}Sr/^{86}Sr$ and reciprocal Sr concentrations (logarithmic scale) of selected river systems compiled from the literature (light blue circles) and end-member data for locations of this study (filled yellow circles). The blue star represents the globally-weighted (by flux) continental runoff as estimated by Peucker-Ehrenbrink and Fiske (2019) with a composition of ~0.104 mg/L Sr and a $^{87}Sr/^{86}Sr$ value of 0.71106. The solid line is the result of linear regression ($R^2 = 0.55$, $p < 0.0001$) including all compiled data ($n = 171$). 95% confidence intervals are shown as dashed black lines. The global seawater Sr isotopic value of ca. 0.70918 is indicated by the grey dotted horizontal line. The Sr concentrations of the Gambia River and upper Volta River plot within the lower range of compiled data, whereas Sr contents of waters in the Sine-Saloum are high, attributable to their high salinity. Other arid systems include the Avon and Murchinson (both situated in Western Australia) with anomalously high Sr contents, but correspondingly higher $^{87}Sr/^{86}Sr$ values. The San Joaquin and Sacramento River (both in California) have exceedingly high Sr concentrations, while northern Australian systems (particularly Marrakai Creek) exhibit comparably low Sr contents but highly radiogenic isotopic values. It is noted that data in this compilation were obtained during distinct seasons and stages of rivers. The data can be found in Table S1

placed alongside rivers that primarily drain Phanerozoic limestones (high Sr contents, $^{87}Sr/^{86}Sr$ around 0.710; C. E. Jones and Jenkyns 2001). The only two systems with higher Sr concentrations (but low salinities of ≤ 0.2) in our data compilation are the adjoining Sacramento River (95 mg/L; $^{87}Sr/^{86}Sr = 0.70576$) and San Joaquin River (209 mg/L; $^{87}Sr/^{86}Sr = 0.70714$) in California, USA (Hobbs et al. 2019), which drain young volcanic terrain and marine precipitates (Ingram and Weber 1999).

Conclusions

Water and catfish otolith samples from three modern estuaries in NW Africa revealed distinct systematics of $^{87}Sr/^{86}Sr$, Sr concentrations, and salinity, altogether reflecting the predominant control of the geological context and hydrology of the drainage basin on the Sr geochemistry of water. In the Gambia River, water exhibited a strong correspondence between theoretically and empirically determined relationships of $^{87}Sr/^{86}Sr$ and salinity, demonstrating the potential of $^{87}Sr/^{86}Sr$ as a quantitative proxy when Sr behaves conservatively, and seawater and freshwater end-members contributing to estuarine mixing are isotopically distinct and well-characterised. Calculated and observed $^{87}Sr/^{86}Sr$ relationships of water in the Volta estuary were likewise correlated, but showed larger discrepancies, potentially linked to an additional unknown source of Sr to the water. $^{87}Sr/^{86}Sr$ measurements of catfish otoliths from both estuaries clearly depicted a combined influence of respective freshwater and seawater end-members, and served to demonstrate that the reliability of $^{87}Sr/^{86}Sr$-based salinity reconstructions is best at low salinities. At higher salinities, an optimisation of the analytical procedure may improve the resolution of the proxy, which is ultimately restricted by instrumental reproducibility. However, localised departures from linear mixing behaviour in the Volta River highlight the necessity of sampling across the estuarine gradient instead of relying on single measurements of end-member compositions to confirm model assumptions

and prevent potential misinterpretations. Our pilot study encourages additional water sampling in these two estuaries at different times of the year and at higher spatial coverage to substantiate and refine quantitative relationships between $^{87}Sr/^{86}Sr$ and salinity. The excellent preconditions and pristine ecological state of the Gambia River in particular, strongly support the use of this approach for high-resolution (ontogenetic) geochemical fingerprinting to help unravel the life-histories of key NW African fish species with view to informing conservation efforts. In the hypersaline Sine-Saloum, large inconsistencies in the Sr geochemistry of water and otoliths highlighted how excessive evaporation violates fundamental assumptions for mixing models, altogether precluding the establishment of quantitative mixing lines. Nonetheless, we emphasise the opportunity for palaeoenvironmental investigations in the Sine-Saloum and other (palaeo-)estuaries (e.g., the Banc d'Arguin, Mauritania), using fossil carbonate structures from shell-midden deposits that predate the estuary's salinity inversion, and may serve as valuable archives of the NW African climate evolution well into the mid-Holocene.

Supplementary Information The online version contains supplementary material available at https://doi.org/10.1007/s12237-021-01041-x.

Acknowledgements We thank the following people for their assistance and support: Sebastian Flotow (ZMT) for sample preparation; Jule Mawick (ZMT) for elemental analysis; Dr. Thomas Mann (ZMT) and Jan Schuster (Kommunale Entwicklungspolitik, Stadt Eschweiler) for assistance with organisation and logistics; Dr. Khady Diouf Goudiaby (Université Cheikh Anta Diop, Institut Fondamental d'Afrique Noir; IFAN) for helpful discussions of otolith collection and interpretation. We acknowledge the AWA project "Ecosystem Approach to the management of fisheries and the marine environment in West African waters" funded by the BMBF and IRD (grant agreement 01DG12073E) for encouraging collaborative research between European and West African countries. We further acknowledge previous joint research efforts between the IRD (UR RAP, Dakar) and the Gambian Fisheries Department for networking. On behalf of all co-authors, we thank Jill Olin, Malte Willmes, and two anonymous reviewers for their constructive feedback and suggestions, which significantly improved our manuscript.

Funding Open Access funding enabled and organized by Projekt DEAL.

Data Availability Datasets generated in this study havebeen submitted to PANGAEA Data Publisher. Refer to the electronicversion of this article for the updated DOI link to the data.

References

Albaret, J.J., M. Simier, F.S. Darboe, J.-M. Ecoutin, J. Raffray, and L.T. de Morais. 2004. Fish diversity and distribution in the Gambia Estuary, West Africa, in relation to environmental variables. *Aquatic Living Resources* 17 (1): 35–46.

Ando, A., T. Nakano, H. Kawahata, Y. Yokoyama, and B.-K. Khim. 2010. Testing seawater Sr isotopic variability on a glacial-interglacial timescale: An application of latest high-precision thermal ionization mass spectrometry. *Geochemical Journal* 44 (5): 347–357.

Azzoug, M., M. Carré, B.M. Chase, A. Deme, A. Lazar, C.E. Lazareth, A.J. Schauer, M. Mandeng-Yogo, M. Simier, A. Thierno-Gaye, and L.T. de Morais. 2012. Positive precipitation-evaporation budget from AD 460 to 1090 in the Saloum Delta (Senegal) indicated by mollusk oxygen isotopes. *Global and Planetary Change* 98–99: 54–62.

Ba, K., M. Thiaw, M. Fall, N. Thiam, B. Meissa, D. Jouffre, O. T. Thiaw, and D. Gascuel. 2018. Long-term fishing impact on the Senegalese coastal demersal resources: diagnosing from stock assessment models. *Aquatic Living Resources* 31 (8).

Banner, J.L. 2004. Radiogenic isotopes: systematics and applications to earth surface processes and chemical stratigraphy. *Earth-Science Reviews* 65: 141–194.

Barusseau, J.-P., M. Bă, C. Descamps, E. Salif Diop, B. Diouf, A. Kane, J.L. Saos, and A. Soumaré. 1998. Morphological and sedimentological changes in the Senegal River estuary after the constuction of the Diama dam. *Journal of African Earth Sciences* 26 (2): 317–326.

Bataille, C.P., J. Laffoon, and G.J. Bowen. 2012. Mapping multiple source effects on the strontium isotopic signatures of ecosystems from the circum-Caribbean region. *Ecosphere* 3 (12): 118.

Beard, B.L., and C.M. Johnson. 2000. Strontium isotope composition of skeletal material can determine the birth place and geographic mobility of humans and animals. *Journal of Forensic Science* 45 (5): 1049–1061.

Beck, A.J., M.A. Charette, J.K. Cochran, M.E. Gonneea, and B. Peucker-Ehrenbrink. 2013. Dissolved strontium in the subterranean estuary - Implications for the marine strontium isotope budget. *Geochimica Et Cosmochimica Acta* 117: 33–52.

Blum, J.D., and Y. Erel. 2003. Radiogenic isotopes in weathering and hydrology. *Treatise on Geochemistry* 5: 605.

Brennan, S.R., C.E. Zimmerman, D.P. Fernandez, T.E. Cerling, M.V. McPhee, and M.J. Wooller. 2015. Strontium isotopes delineate fine-scale natal origins and migration histories of Pacific salmon. *Science Advances* 1 (4): e1400124.

Brochier, T., J.-M. Ecoutin, L.T. De Morais, D.M. Kaplan, and R. Laë. 2013. A multi-agent ecosystem model for studying changes in a tropical estuarine fish assemblage within a marine protected area. *Aquatic Living Resources* 26 (2): 147–158.

Burke, W.H., R.E. Denison, E.A. Hetherington, R.B. Koepnick, H.F. Nelson, and J.B. Otto. 1982. Variation of seawater $^{87}Sr/^{86}Sr$ throughout Phanerozoic time. *Geology* 10 (10): 516–519.

Campana, S.E. 1999. Chemistry and composition of fish otoliths: Pathways, mechanisms and applications. *Marine Ecology Progress Series* 188: 263–297.

Campana, S.E., G.A. Chouinard, J.M. Hanson, A. Frechet, and J. Brattey. 2000. Otolith elemental fingerprints as biological tracers of fish stocks. *Fisheries Research* 46 (1–3): 343–357.

Capo, R.C., B.W. Stewart, and O.A. Chadwick. 1998. Strontium isotopes as tracers of ecosystem processes: Theory and methods. *Geoderma* 82 (1): 197–225.

Castro, K., A. Jallow, and S. Cessay. 2013. Description and analysis of the Gambia catfish stock assessment 2013. Retrieved from https://www.crc.uri.edu/download/GambiaCatfish_stock_assessment508.pdf (September 2021).

Chang, C.-W., S.-H. Lin, Y. Iizuka, and W.-N. Tzeng. 2004. Relationship between Sr: Ca ratios in otoliths of grey mullet Mugil cephalus and ambient salinity: Validation, mechanisms, and applications. *Zoological Studies* 43 (1): 74–85.

Conand, F., S.B. Camara, and F. Domain. 1995. Age and growth of three species of Ariidae (siluriformes) in coastal waters of Guinea. *Bulletin of Marine Science* 56 (1): 58–67.

Conrad, G., and J.-R. Lappartient. 1987. Le 'continental terminal', sa place dans l'évolution géodynamique du bassin sénégalo-mauritanien durant le Cénozoïque. *Journal of African Earth Sciences (1983)* 6 (1): 45–60.

Crook, D.A., K. Lacksen, A.J. King, D.J. Buckle, S.J. Tickell, J.D. Woodhead, R. Maas, S.A. Townsend, and M.M. Douglas. 2016. Temporal and spatial variation in strontium in a tropical river: Implications for otolith chemistry analyses of fish migration. *Canadian Journal of Fisheries and Aquatic Sciences* 74 (4): 533–545.

Crook, D.A., D. Wedd, and T.M. Berra. 2015. Analysis of otolith $^{87}Sr/^{86}Sr$ to elucidate salinity histories of Nurseryfish *Kurtus gulliveri* (Perciformes: Kurtidae) in a tropical lowland river in northern Australia. *Freshwater Science* 34: 609–619.

Crowley, B.E., J.H. Miller, and C.P. Bataille. 2017. Strontium isotopes ($^{87}Sr/^{86}Sr$) in terrestrial ecological and palaeoecological research: Empirical efforts and recent advances in continental-scale models. *Biological Reviews* 92 (1): 43–59.

Dankwa, H.R., and C. Gordon. 2002. The fish and fisheries of the Lower Volta mangrove swamps in Ghana. *African Journal of Science and Technology* 3 (1): 25–32.

DeBord, J., A. Pourmand, S.C. Jantzi, S. Panicker, and J. Almirall. 2017. Profiling of heroin and assignment of provenance by $^{87}Sr/^{86}Sr$ isotope ratio analysis. *Inorganica Chimica Acta* 468: 294–299.

Degeorges, A., and B.K. Reilly. 2006. Dams and large scale irrigation on the Senegal River: Impacts on man and the environment. *International Journal of Environmental Studies* 63 (5): 633–644.

Deniel, C., and C. Pin. 2001. Single-stage method for the simultaneous isolation of lead and strontium from silicate samples for isotopic measurements. *Analytica Chimica Acta* 426 (1): 95–103.

Descroix, L., Y. Sané, M. Thior, S.-P. Manga, B.D. Ba, J. Mingou, V. Mendy, S. Coly, A. Dièye, A. Badiane, M.-J. Senghor, A.-B. Diedhiou, D. Sow, Y. Bouaita, S. Soumaré, A. Diop, B. Faty, B.A. Sow, E. Machu, J.-P. Montoroi, J. Andrieu, and J.-P. Vandervaere. 2020. Inverse Estuaries in West Africa: Evidence of the Rainfall Recovery? *Water* 12: 647.

De Villiers, S. 2005. Rapid communication. The correct use of Sr isotopes in river-groundwater mixing models: A Breede River case study. *Water SA* 31 (3): 397–398.

Diop, K., K. Diouf, M.D. Ndione, H.D. Diadhiou, M. Thiaw, P. Ndiaye, and D. Jouffre. 2017. Study comparing the reproductive traits of the catfish, *Arius latiscutatus* (Günther, 1864) inside and outside the bamboung marine protected area, Saloum Delta, Senegal. *International Journal of Fisheries and Aquatic Studies* 5 (4): 91–99.

Doumouya, F., A. Diaw, B. Sambou, M. Sadio, H. Sambou, V. Traore, A. Beye, and A. Ali. 2016. Rainfall Variability in Sine Saloum River Basin in a Context of Climate Change and Variability. *Advances in Research* 6 (6): 1–12.

Elderfield, H. 1986. Strontium isotope stratigraphy. *Palaeogeography, Palaeoclimatology, Palaeoecology* 57 (1): 71–90.

Elliot, M., K. Welsh, C. Chilcott, M. McCulloch, J. Chappell, and B. Ayling. 2009. Profiles of trace elements and stable isotopes derived from giant long-lived *Tridacna gigas* bivalves: Potential applications in paleoclimate studies. *Palaeogeography, Palaeoclimatology, Palaeoecology* 280 (1): 132–142.

El Meknassi, S., G. Dera, T. Cardone, M. De Rafélis, C. Brahmi, and V. Chavagnac. 2018. Sr isotope ratios of modern carbonate shells: Good and bad news for chemostratigraphy. *Geology* 46 (11): 1003–1006.

El Meknassi, S., G. Dera, M. De Rafélis, C. Brahmi, F. Lartaud, F. Hodel, C. Jeandal, L. Menjot, S. Mounic, M. Henry, P. Besson, and V. Chavagnac. 2020. Seawater $^{87}Sr/^{86}Sr$ ratios along continental margins: Patterns and processes in open and restricted shelf domains. *Chemical Geology 558.*

Fagade, S.O. 1980. The morphology of the otoliths of the Bagrid catfish, *Chrysichthys nigrodigitatus* (Lacepède) and their use in age determinations. *Hydrobiologica* 71: 209–215.

Farrell, J.W., S.C. Clemens, and P.L. Gromet. 1995. Improved chronostratigraphic reference curve of late Neogene seawater $^{87}Sr/^{86}Sr$. *Geology* 23 (5): 403–406.

Faure, G. 1986. *Principles of Isotope Geology*, 2nd ed. New York: Wiley.

Faure, G., and T.M. Mensing. 2005. *Isotopes: Principles and Applications*, 3rd ed. New York: Wiley.

Faye, S., M.I. Ba, M. Diaw, and S. Ndoye. 2010. The groundwater geochemistry of the Saloum delta aquifer: Importance of silicate weathering, recharge and mixing processes. *African Journal of Environmental Science and Technology* 4 (12): 815–830.

Faye, W., A.N. Fall, D. Orange, F. Do, O. Roupsard, and A. Kane. 2020. Climatic variability in the Sine-Saloum basin and its impacts on water resources: Case of the Sob and Diohine watersheds in the region of Niakhar. *Proceedings of the International Association of Hydrological Sciences* 383: 391–399.

Faye, B., D. Tine, N. Dethié, D. Cheikh, G. Faye, and A. Ndiaye. 2019. Évolution des terres salées dans le nord de l'estuaire du Saloum (Sénégal). *Géomorphologie: Relief, Processus, Environnement* 25 (2): 81–90.

Flecker, R., S. de Villiers, and R.M. Ellam. 2002. Modelling the effect of evaporation on the salinity–$^{87}Sr/^{86}Sr$ relationship in modern and ancient marginal-marine systems: The Mediterranean Messinian Salinity Crisis. *Earth and Planetary Science Letters* 203 (1): 221–233.

Flockhart, D.T.T., T.K. Kyser, D. Chipley, N.G. Miller, and D.R. Norris. 2015. Experimental evidence shows no fractionation of strontium isotopes ($^{87}Sr/^{86}Sr$) among soil, plants, and herbivores: Implications for tracking wildlife and forensic science. *Isotopes in Environmental and Health Studies* 51 (3): 372–381.

Freitas, P.S., L.J. Clarke, H. Kennedy, C.A. Richardson, and F. Abrantes. 2006. Environmental and biological controls on elemental (Mg/Ca, Sr/Ca and Mn/Ca) ratios in shells of the king scallop *Pecten maximus*. *Geochimica Et Cosmochimica Acta* 70 (20): 5119–5133.

Gao, Y., J. Petersen, R. Conrad, and D.L. Dettman. 2015. Isotopic differences between the left and right side otoliths of flatfish indicating growth rather than environment. *Fisheries and Aquaculture Journal* 6 (1): 1.

Gillanders, B.M. 2005. Otolith chemistry to determine movements of diadromous and freshwater fish. *Aquatic Living Resources* 18: 291–300.

Gillikin, D. P., A. Lorrain, J. Navez, J. W. Taylor, L. André, E. Keppens, W. Baeyens, and F. Dehairs. 2005. Strong biological controls on Sr/Ca ratios in aragonitic marine bivalve shells. *Geochemistry, Geophysics, Geosystems* 6 (5).

Goldstein, S.J., and S.B. Jacobsen. 1987. The Nd and Sr isotopic systematics of river-water dissolved material: Implications for the

sources of Nd and Sr in seawater. *Chemical Geology: Isotope Geoscience Section* 66 (3–4): 245–272.

Hardy, K., A. Camara, R. Piqué, E. Dioh, M. Guèye, H.D. Diadhiou, M. Faye, and M. Carré. 2016. Shellfishing and shell midden construction in the Saloum Delta, Senegal. *Journal of Anthropological Archaeology* 41: 19–32.

Hobbs, J.A., L.S. Lewis, N. Ikemiyagi, T. Sommer, and R.D. Baxter. 2010. The use of otolith strontium isotopes ($^{87}Sr/^{86}Sr$) to identify nursery habitat for a threatened estuarine fish. *Environmental Biology of Fishes* 89 (3–4): 557–569.

Hobbs, J.A., L.S. Lewis, M. Willmes, C. Denney, and E. Bush. 2019. Complex life histories discovered in a critically endangered fish. *Scientific Reports* 9 (1): 16772.

Hodell, D.A., R.L. Quinn, M. Brenner, and G. Kamenov. 2004. Spatial variation of strontium isotopes ($^{87}Sr/^{86}Sr$) in the Maya region: A tool for tracking ancient human migration. *Journal of Archaeological Science* 31 (5): 585–601.

Holmden, C., and J.D. Hudson. 2003. $^{87}Sr/^{86}Sr$ and Sr/Ca Investigation of Jurassic mollusks from Scotland: Implications for paleosalinities and the Sr/Ca ratio of seawater. *Bulletin of the Geological Society of America* 115 (10): 1249–1264.

Höpker, S.N., H.C. Wu, P. Müller, J.-P. Barusseau, R. Vernet, F. Lucassen, S.A. Kasemann, and H. Westphal. 2019. Pronounced Northwest African Monsoon Discharge During the Mid- to Late Holocene. *Frontiers in Earth Science* 7: 314.

Huang, K., C. You, C. Chung, and I. Lin. 2011. Nonhomogeneous seawater Sr isotopic composition in the coastal oceans: A novel tool for tracing water masses and submarine groundwater discharge. *Geochemistry, Geophysics, Geosystems* 12 (5).

Ingram, B.L., and D. Sloan. 1992. Strontium isotopic composition of estuarine sediments as paleosalinity-paleoclimate indicator. *Science* 255 (5040): 68–72.

Ingram, B.L., and P.K. Weber. 1999. Salmon origin in California's Sacramento-San Joaquin river system as determined by otolith strontium isotopic composition. *Geology* 27 (9): 851–854.

Jones, C.E., and H.C. Jenkyns. 2001. Seawater strontium isotopes, oceanic anoxic events, and seafloor hydrothermal activity in the Jurassic and Cretaceous. *American Journal of Science* 301: 112–149.

Jones, M.T., S.R. Gislason, K.W. Burton, C.R. Pearce, V. Mavromatis, P.A.E. Pogge von Strandmann, and E.H. Oelkers. 2014. Quantifying the impact of riverine particulate dissolution in seawater on ocean chemistry. *Earth and Planetary Science Letters* 395: 91–100.

Jørgensen, N.O., and B. Banoeng-Yakubo. 2001. Environmental isotopes (^{18}O, ^{2}H, and $^{87}Sr/^{86}Sr$) as a tool in groundwater investigations in the Keta Basin, Ghana. *Hydrogeology Journal* 9: 190–201.

Kennedy, B.P., A. Klaue, J.D. Blum, C.L. Folt, and K.H. Nislow. 2002. Reconstructing the lives of fish using Sr isotopes in otoliths. *Canadian Journal of Fisheries and Aquatic Sciences* 59 (6): 925–929.

Kumar, A., W. Abouchami, S.J.G. Galer, V.H. Garrison, E. Williams, and M.O. Andreae. 2014. A radiogenic isotope tracer study of transatlantic dust transport from Africa to the Caribbean. *Atmospheric Environment* 82: 130–143.

Laë, R., J.-M. Ecoutin, A. Mendy, J. Raffray, J.-Y. Weigel, O. Sadio, and O. Djobe. 2004. Effects of a targeted shrimp (*Penaeus notialis*) exploitation on fish catches in the Gambia estuary. *Aquatic Living Resources* 17 (1): 75–85.

Lécorché, J.P., G. Bronner, R.D. Dallmeyer, G. Rocci, and J. Roussel. 1991. The Mauritanide orogen and its northern extensions (western Sahara and Zemmour), West Africa. In *The West African orogens and circum-atlantic correlatives*, ed. R.D. Dallmeyer and J.P. Lécorché, 187–227. Berlin, Heidelberg: Springer.

Lesack, L.F.W., R.E. Hecky, and J.M. Melack. 1984. Transport of carbon, nitrogen, phosphorus, and major solutes in the Gambia River, West Africa. *Limnology and Oceanography* 29 (4): 816–830.

Liu, Y.-W., S.M. Aciego, and A.D. Wanamaker. 2015. Environmental controls on the boron and strontium isotopic composition of aragonite shell material of cultured *Arctica islandica*. *Biogeosciences* 12 (11): 3351–3368.

Logah, F.Y., A.B. Amisigo, E. Obuobie, and K. Kankam-Yeboah. 2017. Floodplain hydrodynamic modelling of the Lower Volta River in Ghana. *Journal of Hydrology: Regional Studies* 14: 1–9.

Loher, T., S. Wischniowski, and G.B. Martin. 2008. Elemental chemistry of left and right sagittal otoliths in a marine fish *Hippoglossus stenolepis* displaying cranial asymmetry. *Journal of Fish Biology* 73 (4): 870–887.

Louca, V., S.W. Lindsay, S. Majambere, and M.C. Lucas. 2009. Fish community characteristics of the lower Gambia River floodplains: A study in the last major undisturbed West African river. *Freshwater Biology* 54: 254–271.

Marcano, M.C., S. Mukasa, K.C. Lohmann, C. Stefano, M. Taviani, and A. Andronikov. 2009. Chronostratigraphic and paleoenvironmental constraints derived from the $^{87}Sr/^{86}Sr$ and $\delta^{18}O$ signal of Miocene bivalves, Southern McMurdo Sound, Antarctica. *Global and Planetary Change* 69 (3): 124–132.

Marceniuk, A. P., and N. A. Menezes. 2007. Systematics of the family Ariidae (Ostariophysi, Siluriformes), with a redefinition of the genera. *Zootaxa* (1416).

McArthur, J.M., R.J. Howarth, and T.R. Bailey. 2001. Strontium isotope stratigraphy : LOWESS version 3: best fit to the marine Sr-isotope curve for 0–509 Ma and accompanying look-up table for deriving numerical age. *The Journal of Geology* 109 (2): 155–170.

Meybeck, M., H.M. Lô, G. Cauwet, and J.-Y. Gac. 1987. Geochemistry of the sahelian Gambia river during the 1983 high-water stage. *Mitteilungen Geologisches Paläontologisches Institüt Universiteit Hamburg* 64: 461–473.

Meyer, I., G.R. Davies, and J.B.W. Stuut. 2011. Grain size control on Sr - Nd isotope provenance studies and impact on paleoclimate reconstructions: An example from deep - sea sediments offshore NW Africa. *Geochemistry, Geophysics, Geosystems* 12 (3): 1–14.

Mikhailov, V.N., and M.V. Isupova. 2008. Hypersalinization of river estuaries in West Africa. *Water Resources* 35 (4): 367–385.

Modestou, S., D. Simon, M. Gutjahr, A. Marzocchi, T.J. Kouwenhoven, R.M. Ellam, and R. Flecker. 2017. Precessional variability of $^{87}Sr/^{86}Sr$ in the late Miocene Sorbas Basin: An interdisciplinary study of drivers of interbasin exchange. *Paleoceanography* 35: 531–552.

Mohan, J.A., R. Rulifson, D.R. Corbett, and N.M. Halden. 2012. Validation of oligohaline elemental otolith signatures of striped bass by use of in situ caging experiments and water chemistry. *Marine and Coastal Fisheries* 4 (1): 57–70.

Mokadem, F., I.J. Parkinson, E.C. Hathorne, P. Anand, J.T. Allen, and K.W. Burton. 2015. High-precision radiogenic strontium isotope measurements of the modern and glacial ocean: Limits on glacial–interglacial variations in continental weathering. *Earth and Planetary Science Letters* 415: 111–120.

Ndehedehe, C.E., J.L. Awange, M. Kuhn, N.O. Agutu, and Y. Fukuda. 2017. Analysis of hydrological variability over the Volta river basin using in-situ data and satellite observations. *Journal of Hydrology: Regional Studies* 12: 88–110.

Nelson, T.R., and S.P. Powers. 2020. Elemental concentrations of water and otoliths as salinity proxies in a northern Gulf of Mexico estuary. *Estuaries and Coasts* 43: 843–864.

Nyekodzi, G., E.T. Lawson, and C. Gordon. 2018. Evaluating the impacts of dredging and saline water intrusion on rural

livelihoods in the Volta Estuary. *International Journal of River Basin Management* 16 (1): 93–105.

Okyere, I., and E.E. Boahemaa-Kobil. 2020. Occurrence and food habits of the bagrid catfish *Chrysichthys nigrodigitatus* (Lacepède, 1803) in the Pra River Estuary, Ghana. *Journal of Fisheries and Coastal Management* 1: 29–34.

Palmer, M.R., and J.M. Edmond. 1989. The strontium isotope budget of the modern ocean. *Earth and Planetary Science Letters* 92 (1): 11–26.

Panfili, J., A.M. Darnaude, L. Vigliola, A. Jacquart, M. Labonne, and S. Gilles. 2015. Experimental evidence of complex relationships between the ambient salinity and the strontium signature of fish otoliths. *Journal of Experimental Marine Biology and Ecology* 467: 65–70.

Panfili, J., D. Thior, J.-M. Ecoutin, P. Ndiaye, and J.-J. Albaret. 2006. Influence of salinity on the size at maturity for fish species reproducing in contrasting West African estuaries. *Journal of Fish Biology* 69: 95–113.

Peros, M.C., E.G. Reinhardt, H.P. Schwarcz, and A.M. Davis. 2007. High-resolution paleosalinity reconstruction from Laguna de la Leche, north coastal Cuba, using Sr, O, and C isotopes. *Palaeogeography, Palaeoclimatology, Palaeoecology* 245 (3–4): 535–550.

Persits, F., T. Ahlbrandt, M. Tuttle, R. Charpentier, M. Brownfield, and K. Takahashi. 2002. Map showing geology, oil and gas fields and geological provinces of Africa, Ver. 2.0. *USGS Open File Report 97–470 A*. Reston: U.S. Geological Survey.

Petr, T. 1986. The Volta river system. In *The ecology of river systems*, ed. B.R. Davies and K.F. Walker, 163–199. Dordrecht: Springer.

Peucker-Ehrenbrink, B., and G.J. Fiske. 2019. A continental perspective of the seawater $^{87}Sr/^{86}Sr$ record: A review. *Chemical Geology* 510: 140–165.

Phillis, C.C., D.J. Ostrach, B.L. Ingram, and P.K. Weber. 2011. Evaluating otolith Sr/Ca as a tool for reconstructing estuarine habitat use. *Canadian Journal of Fisheries and Aquatic Sciences* 68 (2): 360–373.

Poulain, C., D.P. Gillikin, J. Thébault, J.M. Munaron, M. Bohn, R. Robert, Y.M. Paulet, and A. Lorrain. 2015. An evaluation of Mg/Ca, Sr/Ca, and Ba/Ca ratios as environmental proxies in aragonite bivalve shells. *Chemical Geology* 396: 42–50.

Reinhardt, E.G., J. Blenkinsop, and R.T. Patterson. 1998. Assessment of a Sr isotope vital effect ($^{87}Sr/^{86}Sr$) in marine taxa from Lee Stocking Island, Bahamas. *Geo-Marine Letters* 18 (3): 241–246.

Rahaman, W., and S.K. Singh. 2012. Sr and $^{87}Sr/^{86}Sr$ in estuaries of western India: Impact of submarine groundwater discharge. *Geochimica Et Cosmochimica Acta* 85: 275–288.

Santos, R.V., F. Sondag, G. Cochonneau, C. Lagane, P. Brunet, K. Hattingh, and J.G.S. Chaves. 2014. Source area and seasonal $^{87}Sr/^{86}Sr$ variations in rivers of the Amazon basin. *Hydrological Processes* 29 (1): 187–197.

Sarré, A., J.-O. Krakstad, P. Brehmer, and E.M. Mbye. 2018. Spatial distribution of main clupeid species in relation to acoustic assessment surveys in the continental shelves of Senegal and The Gambia. *Aquatic Living Resources* 31: 9.

Scaffidi, B.K., T.A. Tung, G. Gordon, A.K. Alaica, L.M. González La Rosa, S.J. Marsteller, A. Dahlstedt, E. Schach, and K.J. Knudson. 2020. Drinking locally: A water $^{87}Sr/^{86}Sr$ isoscape for geolocation of archaeological samples in the Peruvian Andes. *Frontiers in Ecology and Evolution* 8: 281.

Schneider, W. 1990. FAO species identification sheets for fishery purposes. Field guide to the commercial marine resources of the Gulf of Guinea. *Prepared and published with the support of the FAO Regional Office for Africa, 1–268.* Rome: FAO.

Sessa, J.A., L.C. Ivany, T.H. Schlossnagle, S.D. Samson, and S.A. Schellenberg. 2012. The fidelity of oxygen and strontium isotope values from shallow shelf settings: Implications for temperature and age reconstructions. *Palaeogeography, Palaeoclimatology, Palaeoecology* 342: 27–39.

Shao, Y., J. Farkaš, L. Mosley, J. Tyler, H. Wong, B. Chamberlayne, M. Raven, M. Samanta, C. Holmden, B.M. Gillanders, A. Kolevica, and A. Eisenhauer. 2021. Impact of salinity and carbonate saturation on stable Sr isotopes ($\delta^{88}/^{86}Sr$) in a lagoon-estuarine system. *Geochimica Et Cosmochimica Acta* 293: 461–476.

Simier, M., L. Blanc, C. Aliaume, P.S. Diouf, and J.-J. Albaret. 2004. Spatial and temporal structure of fish assemblages in an "inverse estuary", the Sine Saloum system (Senegal). *Estuarine, Coastal and Shelf Science* 59 (1): 69–86.

Simier, M., C. Laurent, J.-M. Ecoutin, and J.-J. Albaret. 2006. The Gambia River estuary: A reference point for estuarine fish assemblages studies in West Africa. *Estuarine, Coastal and Shelf Science* 69 (3–4): 615–628.

Simier, M., O. J. F. Osse, O. Sadio, and J.-M. Ecoutin. 2021. Biology and ecology of sea catfish (Ariidae) of estuarine, lagoon and coastal ecosystems in West Africa. *Journal of Fish Biology*: 1–15.

Sloterdijk, H., P. Brehmer, O. Sadio, H. Müller, J. Döring, and W. Ekau. 2017. Composition and structure of the larval fish community related to environmental parameters in a tropical estuary impacted by climate change. *Estuarine, Coastal and Shelf Science* 197: 10–26.

Smith, N.G., and C.M. Jones. 2006. Substituting otoliths for chemical analyses: Does sagitta = lapillus? *Marine Ecology Progress Series* 313: 241–247.

Taylor, W. R. (1986). Ariidae. In *Check-List of the freshwater fishes of Africa (CLOFFA),* eds. J. Daget, J.-P. Gosse, and D. F. E. Thys van den Audenaerde. Brussels: Institut Royal des Sciences Naturelles de Belgique.

UNEP (United Nations Environment Programme)-GEF (Global Environment Facility) Volta Project. 2013. *Volta Basin Transboundary Diagnostic Analysis*. UNEP/GEF/Volta/RR 4/2013. Accra, Ghana: UNEP.

Veizer, J., D. Ala, K. Azmy, P. Bruckschen, D. Buhl, F. Bruhn, G.A.F. Carden, A. Diener, S. Ebneth, and Y. Godderis. 1999. $^{87}Sr/^{86}Sr$, $\delta^{13}C$ and $\delta^{18}O$ evolution of Phanerozoic seawater. *Chemical Geology* 161 (1–3): 59–88.

Walther, B.D., and M.K. Niems. 2015. Spatiotemporal variation of trace elements and stable isotopes in subtropical estuaries: I. Freshwater endmembers and mixing curves. *Estuaries and Coasts* 38: 754–768.

Whyte, W. J., and T. S. Russell. 1988. Geological Survey of The Gambia.

Widerlund, A., and P.S. Andersson. 2006. Strontium isotopic composition of modern and Holocene mollusc shells as a palaeosalinity indicator for the Baltic Sea. *Chemical Geology* 232 (1–2): 54–66.

Wierzbowski, H. 2013. Strontium isotope composition of sedimentary rocks and its application to chemostratigraphy and palaeoenvironmental reconstructions. *Annales UMCS, Sectio AAA: PHYSICA* 9: 15.

Zhao, W., W. Balsam, E. Williams, X. Long, and J. Ji. 2018. Sr – Nd – Hf isotopic fingerprinting of transatlantic dust derived from North Africa. *Earth and Planetary Science Letters* 486: 23–31.